Isotopic production cross-sections and recoil velocities of spallation-fission fragments in the reaction ^{238}U(1A GeV)+d

J. Pereira,[1,][*] J. Benlliure,[1] E. Casarejos,[1] P. Armbruster,[2] M. Bernas,[3] A. Boudard,[4] S. Czajkowski,[5] T. Enqvist,[2] R. Legrain,[4] R. Legrain,[4] S. Leray,[4] B. Mustapha,[3] M. Pravikoff,[5] F. Rejmund,[3] K.-H. Schmidt,[2] C. Stéphan,[3] J. Taïeb,[3] L. Tassan-Got,[3] C. Volant,[4] and W. Wlazlo[4]

[1]*Universidad de Santiago de Compostela, Santiago de Compostela E-15782, Spain*
[2]*Gesellschaft für Schwerionenforschung, Darmstadt D-64291, Germany*
[3]*Institute de Physique Nucléaire, Orsay cedex F-91406, France*
[4]*DAPNIA/SPhN, CEA/Saclay, Gif sur Yvette cedex F-91191, France*
[5]*CENBG , Gradignan cedex F-33175, France*
(Dated: March 30, 2006)

Fission fragments of 1A GeV ^{238}U nuclei interacting with a deuterium target have been investigated with the Fragment Separator (FRS) at GSI (Darmstadt) by measuring their isotopic production cross-sections and recoil velocities. The results, along with those obtained recently for spallation-evaporation fragments, provide a comprehensive analysis of the spallation nuclear productions in the reaction ^{238}U(1A GeV)+d. Details about experiment performance, data reduction and results will be presented.

PACS numbers: 21.10.Ft; 21.10.Gv; 25.40.Sc; 25.45.-z; 25.75.-q; 25.85.-w; 29.25.Rm

I. INTRODUCTION

Spallation reactions constitute nowadays one of the most extensively used processes to produce Radioactive Nuclear Beams (RNB's) upon the entire chart of nuclides [1]. Besides their numerous technical and scientific applications (for a review see for instance Refs. [2–6]), these type of reactions have recently turned out to be an optimum tool for investigating the de-excitation of hot nuclei over a wide range of temperatures and fissilities [6–10].

The present paper focuses on the experimental study of the spallation-fission fragments produced in the reaction ^{238}U at 1A GeV with deuterium, and constitutes the complementary part of the analysis of spallation-evaporation fragments presented recently by E.Casarejos et al. [11]. Both experiments are enclosed within an extensive experimental campaign performed at GSI to determine a general inventory of nuclear fragments produced in different spallation reactions [6, 12–23]. The mail goal of the project was the establishment of an extensive benchmark data basis for the design of Accelerator Driven-reactor Systems (ADS) [24, 25] and spallation-neutron sources. A restrictive requirement of these applications is the highly-precise measurement of the isotopic production cross-sections and recoil velocities of spallation-fragments.

The challenging performance of these kind of experiments motivated the use of the inverse-kinematics technique, in which the heavy-ion accelerated at relativistic energies collides with a light-nucleus target in such a way that the spallation-reaction products are emitted forward allowing thus their analysis with an in-flight magnetic separator. At present, the only laboratory offering the possibility of employing such a technique for studying uranium-induced reactions at relativistic energies is the GSI [26] in Darmstadt, Germany. Details about this facility, as well as the experimental technique used to separate and identify the reaction products are presented in the first part of the paper. The second part concerns the data analysis performed to evaluate the recoil velocities and isotopic production cross-sections of the measured fission fragments. The paper ends with a compilation and general discussion of the results. An extensive analysis of these results will be presented in a forthcoming paper.

II. EXPERIMENT

A. Experimental setup

In the present experiment, a ^{238}U primary beam was accelerated in the heavy-ion synchrotron SIS [27] up to an energy of 1A GeV. The intensity, of the order of 10^7 ions/s, was continuously measured during the experiment with the secondary-electron monitor SEE-TRAM [28, 29]. After its extraction, the uranium beam impinged on a cryogenic deuterium target [30] of 201 mg/cm^2 thickness, isolated from the vacuum line by two titanium foils of 18.16 mg/cm^2 thickness each. This target was located at 1.69 m from the entrance of the Fragment Separator (FRS) [31], so that the resulting reaction products were transmitted and measured with the separator before their β-decay. A niobium stripper foil of 60 mg/cm^2 thick was placed downstream the production target in order to maximize the fraction of fully stripped
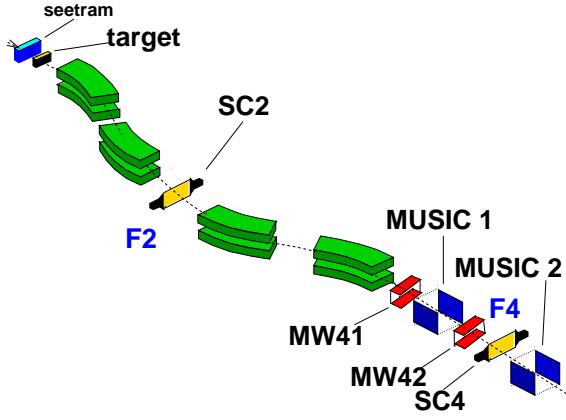
FIG. 1: Schematic view of the FRS with its standard detection equipment.

fragments.

The FRS is an achromatic zero-degree in-flight separator, which consists of four independent stages with their respective image planes (see Fig. 1). The four stages are grouped in two symmetric dispersive areas, so that the entire device remains achromatic. Its high resolving power of 1500, determined for an emittance of 20π mm·mrad and a beam spot of 2.7 mm [31], is achieved at the expenses of a limited acceptance in magnetic rigidity and angle ($\pm1.5\%$ and ±15 mrad, respectively). According to the ion-optics of the FRS, the separation and identification of the fission fragments was performed by combining the signals measured with the standard detection setup shown in Fig. 1:

A pair of plastic scintillators ($SC2$ and $SC4$ [32]), placed at the second (F2) and fourth (F4) image planes were used to determine the horizontal (x direction) deflection of the transmitted nuclei and the time-of-flight from F2 to F4. Two ionization chambers ($MUSIC$'s [33]), placed at the end of the FRS, provided the energy loss of the nuclei. Finally, two multiwires chambers ($MW41$ and $MW42$ [34]) were used to track the transmitted nuclei. All the fast-output signals were filtered by setting the CFD threshold-levels above the electronic noise and the low-amplitude signals generated by light-particles. The trigger for the data-acquisition was given by the signals from the last plastic scintillator ($SC4$). In order to consider a valid event, a software-defined trigger condition required valid position, time-of-flight, angle and energy loss signals.

B. Separation and identification the reaction products with the FRS

1. Separation of transmitted nuclei

The magnetic separation of the nuclides transmitted through the FRS was based upon the relationship between the mass-over-charge ratio A/Z of the nuclei, their

magnetic rigidity $B\rho$, and the longitudinal component of the relativistic reduced momentum $\beta\gamma$:

$$B\rho = \left(\frac{A}{Z}\right) \cdot \frac{m_0}{e} \cdot \beta\gamma \tag{1}$$

being m_0 the nuclear mass unit and e the electron charge.

For a given nucleus, its magnetic rigidity was determined from the horizontal deflection, measured with the plastic scintillator $SC2$ at the dispersive image plane, according to:

$$B\rho = (B\rho)_0 \cdot \left(1 - \frac{x_2}{D_2}\right) \tag{2}$$

where x_2 is the position of the transmitted nucleus, measured in the dispersive plane F2; D_2 is the dispersion at this image plane, corresponding to the first half of the separator; and $(B\rho)_0$ corresponds to the magnetic rigidity of a charged particle following a central trajectory along the FRS. This later quantity was determined by multiplying the magnetic fields of each dipole, measured with Hall probes, with the corresponding curvature radii.

The longitudinal component of the reduced momentum $\beta\gamma$ of the transmitted nuclei (or equivalently their longitudinal velocity v) was calculated by dividing the path length l covered by the ions from F2 to F4 by the time-of-flight ToF between the two plastic scintillators $SC2$ and $SC4$. In order to avoid dependences of the velocity on the angle, an angular correction from the tracking detectors $MW41$ and $MW42$ had to be included in the path-length l.

Together with the mass-over-charge ratio A/Z, we also determined the atomic number of each nuclide, in order to get a full identification. This quantity was deduced from the energy-loss signal ΔE measured with the ionization chambers ($MUSIC's$), corrected for the dependencies on the velocity of the transmitted nuclei and on the horizontal positions of the incoming nuclei at the entrance of the detector with respect to the anodes.

The final resolution attained in the separation of the reaction products is illustrated in the left panel of Fig. 2, where the energy-loss signal is plotted against the mass-over-charge ratio for some selected nuclei. The figure was obtained by summing up all the fission settings measured during the experiment.

As far as the selection of transmitted nuclei is concerned, the transversal dimensions of the inner tubes of the FRS and the maximum magnetic dispersion set a limit on the range of magnetic rigidities accepted by the separator. Assuming a maximum dispersion of -6.8 cm/% at the dispersive image plane, a $B\rho$-acceptance of ±1.5 % was deduced from Eq. 2; those nuclei with magnetic rigidities 1.5% greater or lesser than the central value $(B\rho)_0$ were deflected out to the FRS beam line. This limited range of accepted $B\rho$'s, together with the velocity spread, defined a region of A/Z values that could be measured in one single tuning (setting) of the magnetic dipoles.

Since the nuclei produced in the collision of ^{238}U at 1A GeV with the deuterium target spread out over a wide region of atomic and mass numbers, the FRS had to be adjusted according to the magnetic rigidities of the medium-mass fission fragments to be analyzed. From the calculated values of $B\rho$, a central value $(B\rho)_0$ of the FRS was selected by properly adjusting the magnetic fields of each dipole magnet according to the curvature radii. In order to cover the region of interest, the measurements were repeated for 33 settings centered in different values of $(B\rho)_0$, separated from each other in steps of 1%.

2. Isotopic identification

The identification of the atomic number Z for each nucleus was deduced using the energy-loss signals (ΔE) of the projectile-nucleus as a reference.

The identification of mass numbers was obtained from the matrix $(A/Z) - Z$ (Fig. 2, right): depending on the values of the mass and atomic numbers of the nucleus, the different nuclei are located at different blobs in this matrix. The possible combinations obtained between the quantities A/Z and Z −where Z and A are integer numbers− defined a characteristic pattern in which the nuclei could be grouped within curved lines. The only line with no curvature corresponds to light nuclei with the same number of protons and neutrons ($Z = N$). The next group-line on the right corresponds to nuclei with $N = Z + 1$, which differs a bit from a perfect vertically. If one then goes n steps to the right, the line found corresponds to the group of isotopes with $N = Z + n$. Thus, from the vertical group-line $A = 2Z$ it was possible to identify the mass number of all the nuclides, since their atomic number was well known. The same rule applied to the next lines to the right ($N = Z + 1, N = Z + 2, ...$) in such a way that all the nuclei could be identified in mass A and atomic Z numbers.

Figure 3 shows the identification-matrix obtained by summing up all the different settings measured during the experiment. From this figure, about 1000 different nuclides could be identified.

III. DATA REDUCTION

A. Determination of recoil velocities

The recoil velocities of the fission fragments were evaluated in order to investigate the kinematics associated with the reaction mechanism. The spallation reaction itself is characterized by the collision of a heavy uranium projectile with a deuterium target nucleus, followed by the de-excitation of the projectile-like fragments by fission or by evaporation of light particles. The kinematics of the final fragments correspond to the convolution of the velocity distribution produced by the fast collision, and the subsequent de-excitation processes.

In the present experiment, the kinematics of the fission and evaporation fragment productions were separated by measuring the velocity distribution along the beam axis (hereafter referred to as v), filtered by the limited angular acceptance of the FRS. As discussed in Refs. [18, 35], this limitation truncates the velocity distributions of fission and evaporation fragments in a different manner, in such a way that they could be identified from the resulting measured v-distribution. By making use of Eq. 2, it was possible to determine the longitudinal velocities of the nuclei transmitted through the FRS from their positions at the dispersive image plane (F2) and the identified values of Z and A:

$$v = c \cdot \left\{ \left[\frac{A/Z}{(B\rho)_0 \cdot \left(1 + \frac{x_2}{D_2}\right)} \right]^2 + 1 \right\}^{-1/2} \tag{3}$$

where c refers to the speed of light. In order to determine the exact recoil velocities of the reaction products, the values obtained from Eq. 3 had to be corrected by the energy losses of the transmitted nuclei in the different layers of matter situated between the deuterium target and the plastic scintillator. This correction was done by calculating the energy loss of each nucleus along the flight path from the middle of the target −where the reaction was assumed to take place on average− to the second image plane. Finally, the corrected velocities were transformed into the frame of the projectile.

The accuracy of the velocity determined from Eq. 3 was mainly limited by the position resolution of the plastic scintillator $SC2$, $\Delta x_2 \simeq 2$ mm and the relative resolution of $(B\rho)_0$, of the order of 10^{-4}. These values led to a final relative precision of the velocity of about 3×10^{-4} which proves to be a real achievement when compared with other experimental techniques.

In order to reconstruct the v-distribution of a given nucleus, the contributions measured in different magnetic settings of the FRS were summed up and normalized to the corresponding beam intensities N_{proj}. As an example of this procedure, Fig. 4 depicts the reconstructed velocity spectra for different nuclei as a function of the mass number in form of a scatter plot. The upper and lower wings correspond to the transmitted forward- and backward-emitted fission fragments, respectively, while the central cloud represents the contribution of evaporation. The centroid of this latter distribution is slightly slowed down with respect to the velocity of the projectile, while the two external wings approach each other as the fragment charge increases. The separation between these two wings is related to the fission velocity v_{fiss} and its reduction can be partially attributed to a decrease of the kinetic energy of the two fission partners due to momentum conservation in mass-asymmetric systems and, to a lesser degree, to the weakness of the Coulomb repulsion at large charge-asymmetries. Apart from this, the distribution of fragments produced in the two reaction mechanisms is consistent with theoretical expectations:
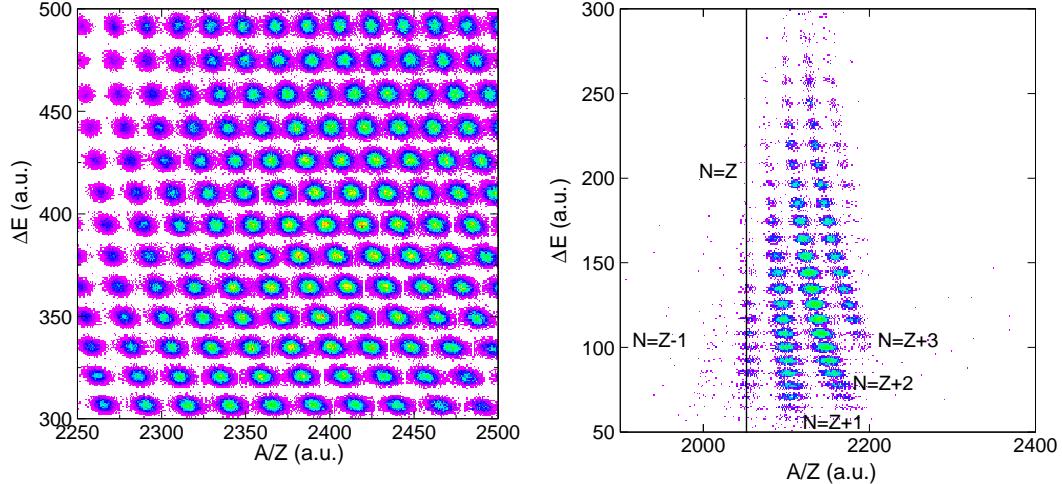
FIG. 2: Two-dimensional cluster plots showing the energy-loss signal against the mass-over-charge ratio. Left: Separated nuclei, represented by the different blobs. Right: Isospin identification (the vertical line corresponds to nuclei with N=Z)

fission fragments are mostly produced with greater neutron excess, while evaporation generally leads to nuclei along the so-called evaporation corridor, located on the neutron-deficient side of the β-stability valley. Furthermore, as the charge of the element increases, the evaporation contribution is enhanced until it becomes the dominant production mechanism.

The velocities of the fission fragments v_{fiss} in the frame of the projectile were obtained for each isotope by fitting the measured velocity spectra to specific functions which reproduced the contribution from each reaction mechanism. Figure 5 depicts an example of the fit obtained for ^{83}Sr. The central peak due to the evaporation component, was described by a Gaussian function $f_{evap}(v)$, while the forward and backward fission peaks were best reproduced by fitting functions defined by the convolution of a Gaussian and an exponential function. Each of these functions $f^f_{fiss}(v)$ and $f^b_{fiss}(v)$ had four free parameters, three of which corresponded to the Gaussian components, while the fourth parameter represented the skewness of the inner tails. The spectra were fitted to a global function $F(v)$ with eleven parameters (three from the Gaussian evaporation component and eight from the forward and backward fit-functions):

$$F(v) = f^b_{fiss}(v) + f_{evap}(v) + f^f_{fiss}(v) \qquad (4)$$

The spectra of isotopes produced only by fission or evaporation were well described by the functions of the specific component, only.

As can be seen in Fig. 6, the radius of the spherical fission distribution, corresponding to the velocity of the fission fragments v_{fiss}, could be obtained by halving the distance between the external sides of the forward and

backward fission peaks, given by v_f and v_b:

$$v_{fiss} = \frac{|v_f - v_b|}{2} = \frac{|v_f| + |v_b|}{2} \qquad (5)$$

However, the determination of v_f and v_b from the velocity spectra was quite complicated due to the smooth side tails of the fission peaks.

Alternatively, the values of v_f and v_b could be expressed as a function of the most probable velocities v_f^{max} and v_b^{max} that corresponded to the maximum of the forward and backward fitting functions $f_f(v)$ and $f_b(v)$, according to:

$$v_f = v_f^{max} + \frac{v_{fiss} - v_{fiss}\cos\alpha_f}{2} \qquad (6)$$

and

$$v_b = v_b^{max} + \frac{v_{fiss} + v_{fiss}\cos\alpha_b}{2} \qquad (7)$$

where α_f and α_b are the forward and backward angles obtained by a Lorentz transformation of the angular acceptance α_{eff} of the FRS into the frame of the fissioning system [35, 36]. These two equations can be re-written as:

$$v_f = v_f^{max} + v_{fiss} \cdot T_f(v_{fiss}) \qquad (8)$$

and

$$v_b = v_b^{max} + v_{fiss} \cdot T_b(v_{fiss}) \qquad (9)$$

where $T_f(v_{fiss})$ and $T_b(v_{fiss})$ are the v_{fiss}-dependent transmissions of the forward- and backward-emitted fission fragments, calculated according to Ref. [35].
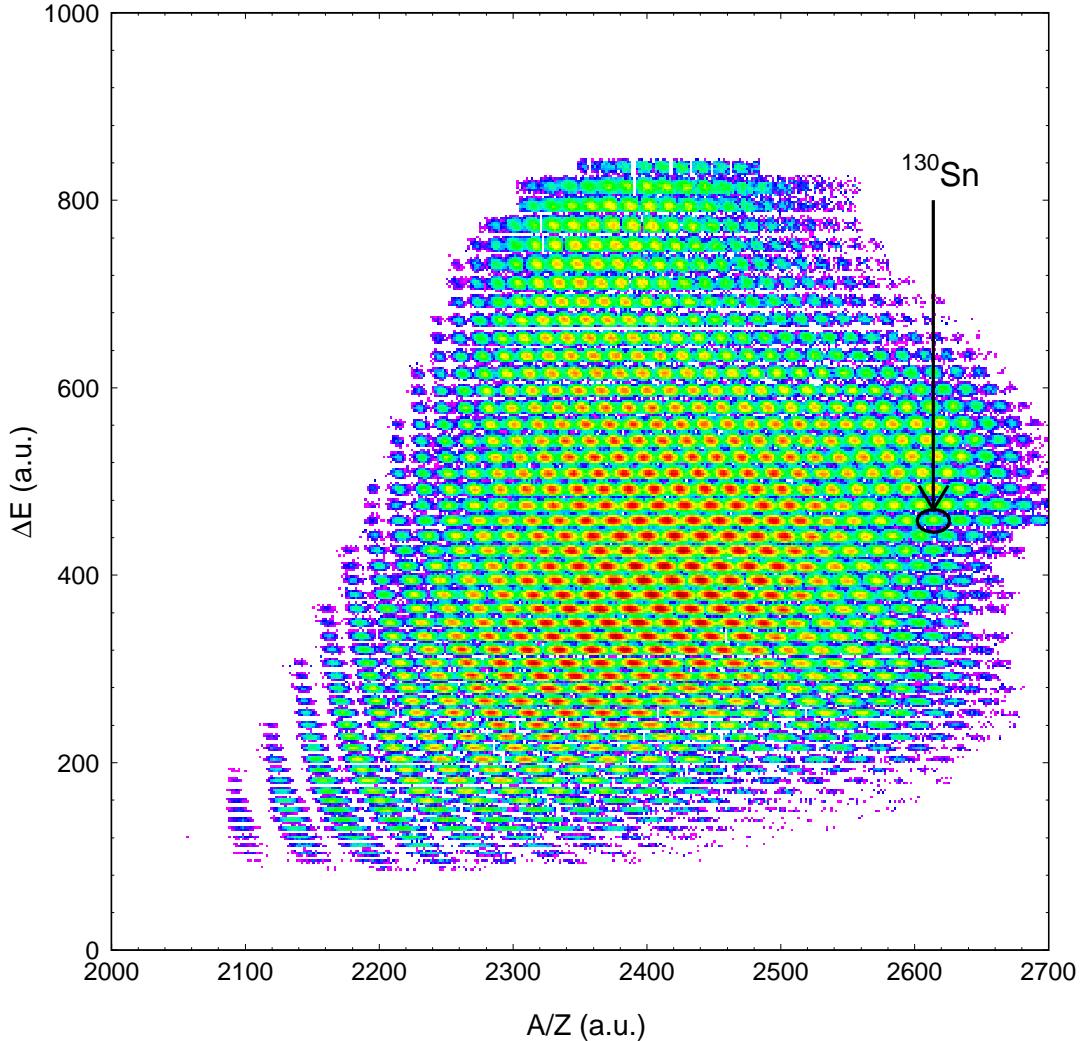
FIG. 3: Identification matrix in form of a scatter plot, showing the atomic number versus the mass-over-charge of all the nuclei measured in 33 different settings of the reaction ^{238}U(1A GeV)+d. As an example, the fission fragment ^{130}Sn is indicated.

The idea behind Eqs. 8 and 9 was that the velocities v_f^{max} and v_b^{max}, obtained from the fitting functions, must be corrected using the fission velocity v_{fiss} and the angular transmission, in order to provide the values v_f and v_b. Because v_{fiss} depends on v_f and v_b (see Eq. 5), and T_f and T_b on v_{fiss}, we used the recursive algorithm described in Ref. [35] to deduce both the forward- and backward-transmissions T_f, T_b, and the fission velocity v_{fiss}. The iterative calculation of the algorithm stops when the measured velocities v_f^{max} and v_b^{max} converges to constant values, which are assumed to correspond to v_f and v_b.

There were two sources of uncertainty in the above-described method: first was the determination of v_f^{max} and v_b^{max} from fits and second was the uncertainty of the angular acceptance value α_{eff} used to calculate T_f and T_b. The former varies considerably from one nucleus to another and depends mainly on the smoothness of the velocity profile; it ranged typically from 1% to 5%, reaching in some particular cases maximum values up to 20%. Concerning the uncertainty due to α_{eff}, it mainly affected the velocities of fragments with rather low transmission. A deep analysis of the ion-optics and the geometry of the FRS yielded a total uncertainty for α_{eff} of about 4% [35], resulting in an uncertainty for the velocities of less than 5%.

Finally, an additional source of error arose from the production of secondary reactions in the deuterium tar-
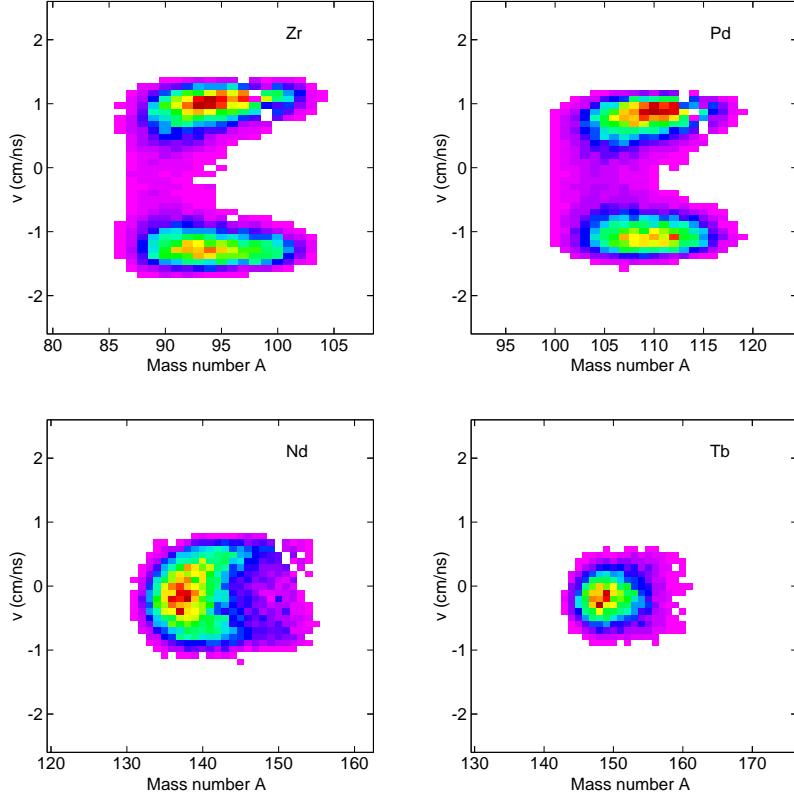
FIG. 4: Scatter plots of $_{40}Zr$, $_{46}Pd$, $_{60}Nd$ and $_{65}Tb$ elements showing the velocity distributions measured in the frame of the projectile as a function of the mass number.
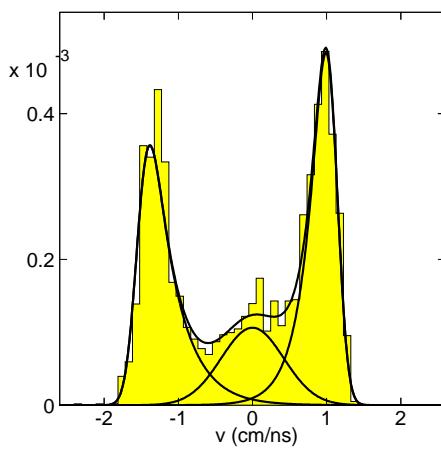
FIG. 5: Velocity-spectrum fit for ^{83}Sr showing the contributions from evaporation (central Gaussian curve) and fission (external curves) to the global fit.

get induced by a heavy primary fission fragment. Such a process would reduce the atomic and mass numbers of the fission fragments, while slightly blurring its ve-

locity spectra. As a consequence, the velocity distribution of the isotope can be partially contaminated by the velocities of the heavier fission fragments that underwent a secondary reaction, thus leading to a reduction of the measured values of v_f^{max} and v_b^{max}, as shown in Ref. [18]. This contamination was only significant for the most neutron-deficient fragments.

B. Determination of production cross-sections

In the thin-target approximation, the total production-yield of a given isotope is defined by:

$$Y_{tot}(Z,A) = \frac{N(Z,A)}{N_{proj}} \qquad (10)$$

where $N(Z,A)$ is the number of nuclei, with a given Z and A, measured during the experiment, and N_{proj} is the number of beam particles. The value of $N(Z,A)$ was obtained by integrating the measured velocity spectra for each nucleus. These spectra were partly contaminated by the fragment production on the titanium windows surrounding the cryogenic deuterium target. In order to subtract the contamination from the reactions produced in the titanium windows, all the measurements
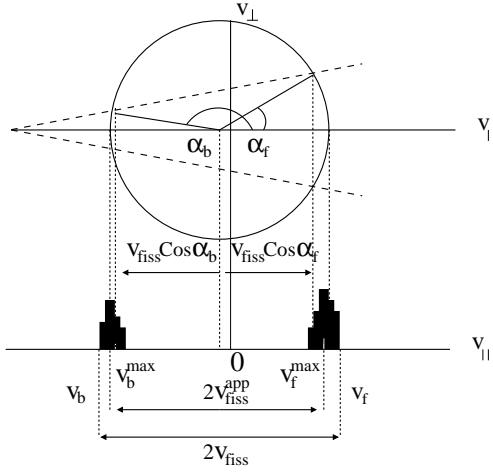
FIG. 6: Schematic representation of the velocity distribution of fission fragments (solid circumference) affected by the cuts produced by the limited angular acceptance of the FRS (dashed lines). (Note the shift of the velocity distribution with respect to the velocity of the projectile, marked by the origin of the reference frame). The projection of the transmitted nuclei onto the axis parallel to the beam direction (longitudinal component) is shown on the lower part of the figure. The measured most-probable forward and backward fission velocities v_f^{max} and v_b^{max} are compared with the real values v_f and v_b.

FIG. 7: Element distribution of fission-fragment production yields in the cryogenic deuterium target Y_{tot} (dots) and the titanium dummy target Y_{dummy} (triangles).

were repeated with a titanium dummy target of thickness equivalent to the target windows. The total yields $Y_{tot}(Z, A)$, integrated over the isotopic chains, are compared in Fig. 7 with the contribution from the titanium dummy target (or equivalently the titanium windows) Y_{dummy}. The production cross-sections for the reaction induced on deuterium were determined from:

$$\sigma_{prod}(Z, A) = \frac{1}{\chi} \cdot [Y_{tot}(Z, A) - Y_{dummy}(Z, A)] \cdot F \quad (11)$$

being χ the density of deuterium nuclei integrated over the target thickness. The factor F includes the different corrections that had to be applied to the measured data due to the limitations of the experimental setup. This factor was calculated according to:

$$F = f_{eff} \cdot f_{sr} \cdot f_{ch} \cdot f_{ev} \cdot f_\tau \quad (12)$$

where f_{eff} accounts for the efficiencies of the experimental setup, f_{sr} corresponds to the corrections that were necessary due to secondary reactions, f_{ch} considers the charge states of the measured nuclei, f_{ev} corrects the contamination from evaporation reactions, and f_τ takes into account the dead time of the data acquisition. The calculation of these correction factors has been extensively described in previous analysis of fission and evaporation fragment productions (see for instance Refs. [6, 12–23]). Consequently, in the present discussion we rather restrict ourself to mention their main features.

The correction due to limitations of the efficiency f_{eff} included the intrinsic efficiency of the detection setup

and the angular transmission of the FRS. The former was evaluated for each element by comparing the total number of valid events with the number of events detected with the $MUSIC's$ detectors (with an efficiency of 100%). The resulting values were above 98% in most of the cases. The correction due to the limited angular transmission of the FRS was evaluated according to the method described in Ref. [35]. This method was based on the calculation of the angular acceptance α_{eff} and the analysis of the fission kinematics. The resulting total angular transmission varied largely from values near 100%, for heavy fragments with rather narrow angular emittance, to values around 15%, for the lightest nuclei. The uncertainty associated with this correction method arose from two different sources, namely the calculation of the angular acceptance α_{eff} and the analysis of the kinematics. The final transmission correction error varied significantly from about 2% to 30%, for some particular cases.

Apart from the primary reactions in the target, the beam particles and the reaction products could undergo further reactions in the different layers of matter placed along the FRS, thereby modifying the primary fragment productions. The list of possible "parasitic" targets included the accelerator window, the aluminum SEE-TRAM foils, the titanium windows surrounding the cryogenic target, a niobium stripper foil behind the target, and the plastic scintillator $SC2$. The probability for a given nucleus to undergo a secondary reaction was estimated by multiplying the production cross sections, obtained from Glauber-type model calculations [37, 38], by the number of impinging beam particles and the number of target nuclei of the corresponding layer. Most of the fragments produced in the aluminum SEETRAM foils and the accelerator window were not transmitted through the FRS due to their large distance with respect

to the entrance of the separator that reduced significantly the value of α_{eff}. This effect, along with the very small thicknesses of these "parasitic" targets led to contributions to the total measured productions of about 5 %. The correction due to secondary reactions induced in the plastic scintillator $SC2$ reached rather low values ranging from 10%, for the lightest elements to almost 20% for the heaviest. Furthermore, the primary fragments produced in the reaction ^{238}U(1A GeV)+d could undergo a secondary reaction before leaving the rather thick deuterium target. These secondary products could also induce a ternary reaction resulting in a multi-step reaction chain. The multiple reaction contaminants did not spread uniformly over the total fragment production but concentrated in some specific regions close to the evaporation corridor. In the case of fission fragments, this contamination mainly affected the neutron-deficient isotopes, gradually increasing as the neutron number decreases. In the present analysis, we used the correction method proposed by P. Napolitani et al. [39]. According to these authors, the measured productions (referred to as apparent cross-sections $\tilde{\sigma}$) were formulated through a system of master equations that included the losses of fragments due to their interaction in the target and the gains due to the contamination from intermediate multiple reactions. A detailed discussion of this model and the underlying approximations used to solve the set of master equations can be found in Ref. [39]. For each given element, the correction factor was found to be constant within 5% to 7% for most of the isotopes, and to drastically drop down when approaching the neutron-deficient side, wherein the corrections reached values close to 100%.

Besides secondary nuclear reactions, the residual nuclei could also pick-up or strip-off some electrons due to the atomic interactions with the different layers of matter. The corresponding fraction of bare ions was maximized by placing a niobium stripper foil of 60 mg/cm^2 thickness behind the target. However, the charge-state configuration of the transmitted ions could change from the first to the second stage of the FRS due to the interactions with the plastic scintillator $SC2$. As explained in Ref. [40], the strong correlation between the charge state of the transmitted ions and their transversal positions at the final image plane makes it possible to discriminate any charge-state change along the FRS. In order to avoid ambiguities in the charge identification, we restricted the present analysis to ions with the same charge-state configuration in both stages. Besides bare ions, this includes hydrogen-like and helium-like ions; though their extremely low fraction (less than 1%) for the range of charges covered by this analysis did not affect the final result. According to this criterion, the losses of measured nuclei which were not fully stripped in the two stages of the FRS had to be corrected. For each nucleus, the correction factor f_{ch} was calculated with the GLOBAL code [41, 42] as the inverse of the probability to be fully stripped along the FRS, i.e. the product of the fractions of bare ions behind the niobium stripper foil (first stage)

and behind the scintillator $SC2$ (second stage), respectively. The resulting correction factor kept always below 10% within the range of elements analyzed in the present work.

Regarding the correction due to the dead time of the data acquisition f_τ, the total number of physical triggers generated by the logic of the experiment and the number of events processed by the data acquisition were counted for each setting with scalers. The ratio between both numbers provided the value of the dead time, which was around 15% for most of the settings. Furthermore, the intensity of the primary beam was checked continuously in order to keep the dead time below 30%.

Finally, since the aim of the present work was the determination of the production cross-sections of fission fragments, we had to disentangle the evaporation-reaction contributions to the measured cross-sections. By comparing the productions of all the fragments produced in the cryogenic deuterium target and the titanium dummy target we saw that the evaporation fragments measured in the former system were mainly produced in the titanium windows. However, after subtracting these contaminants, a small evaporation component was still observed in the reaction ^{238}U(1A GeV)+d for heavy neutron-deficient isotopes. In a former analysis of spallation-evaporation fragments produced in this reaction [11], it was found that these nuclei populated the evaporation corridor situated on the neutron-deficient side of the chart of the nuclides, from uranium isotopes down to elements with atomic numbers about Z=58. Below this value, the evaporation component dropped quickly −though still contributing to the production of the most neutron-deficient isotopes− whereas the fission production increased very fast, specially in the neutron-rich side. Therefore, we expected both reaction mechanisms to coexist in the region of light evaporation fragments, with a transition from evaporation to fission as the neutron number increases. Figure 8 illustrates this trend by showing the velocity spectra of three different cesium isotopes. The lightest and heaviest isotopes were mainly produced by evaporation and fission, respectively, while an intermediate situation was found for ^{125}Cs, wherein a weak evaporation component was strongly mixed with the dominant fission mechanism (see also Ref. [11]).

The evaporation contamination to the measured fission fragments was estimated using a phenomenological model based on the two-step formalism [43]. A Glauber-type Monte-Carlo subroutine [15] was chosen to reproduce the fast interaction between the projectile and target. The evaporation stage was simulated with the statistical de-excitation ABLA code [10, 38] and the PROFI fission mass-distribution subroutine [44]. Details of these codes are well beyond the scope of the present paper; it is sufficient to mention here that the reliability of the calculations in estimating evaporation productions in the region of neutron-deficient heavy nuclei was verified by comparing their results with the evaporation cross-sections measured for some nuclei. Our estimations agreed with
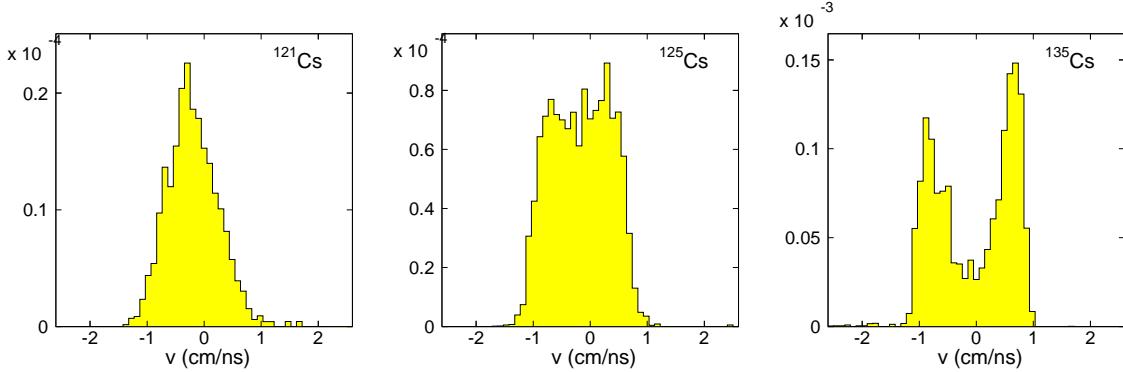
FIG. 8: Measured velocity spectra of three cesium isotopes measured in the reaction ^{238}U(1A GeV)+d.

the experimental results within the precision requirements of the present analysis. Furthermore, the separation method discussed in reference [11] was used in the present analysis for some nuclei and compared with the technique described above. Both methods agreed within their respective uncertainties, thus demonstrating their capabilities to disentangle the two reaction mechanisms.

IV. RESULTS

A. Recoil velocities of fission fragments

Figure 9 shows the velocity distributions of the fission fragments (in the projectile frame) measured in the reaction induced in the deuterium target surrounded by the titanium windows (left) and in the titanium dummy target (right). The distributions were obtained for each element by integrating the contributions of the whole isotopic chain. In the figure, the evaporation fragments lay in a region of velocities close to that of the primary beam, while the forward- and backward-emitted fission fragments correspond to the upper and lower wings. The increase of the fission velocities as the atomic number of the fragments decreases is a natural consequence of the momentum conservation between the light and heavy fission fragments in the frame of the fissioning system.

The recoil velocities v_{fiss} of the fission fragments with atomic numbers ranging from $Z = 23$ to $Z = 66$ were determined according to the method described in section II. Figures 10-12 show the isotopic chains of these recoil velocities v_{fiss} for all the measured fragments. The numerical values, with their associated uncertainties are included in Tabs. I-VIII.

As a general trend, one observes a general reduction of the average fission velocities as the charge of the fission fragments increases. This trend is explained by momentum conservation of the two fission partners: after scission, the total kinetic energy of the system (i.e. the sum of the kinetic energies of each fission partner) comes almost entirely from the Coulomb repulsion between the

two nascent fragments. Due to momentum conservation, the lightest nucleus will acquire more velocity than the heavier one, thus explaining the results shown in the figures.

Regarding the trends observed for a given element the velocities reach a maximum value for the most neutron rich isotopes, then evolve through a plateau for less neutron rich nuclei and finally decrease in the region of light isotopes. This final reduction is more pronounced in the most neutron deficient side with an abrupt decline of v_{fiss} to values 20% below the maximum. The characteristic pattern shown in these figures was already observed in the analysis of fission fragments produced in the reaction ^{238}U (1A GeV)+p [18]. According to this work, the abrupt decrease of the velocities in the neutron-deficient side can be attributed, to some extent, to the contamination of secondary reactions from primary fission fragments. As discussed above, in order to estimate such an effect, we have used the model proposed by P. Napolitani et al. [39]. Those nuclei with a secondary-reaction component greater than 50% are represented in Figs. 10-12 by empty dots. As expected, they correspond to the most neutron-deficient isotopes.

In order to understand the observed isotopic dependence of the recoil velocities, a comparison between the values measured in the present experiment and those obtained from the scission-model developed by Wilkins et al. [45] is shown in Figs. 10-12. The different lines drawn on top of the experimental values correspond to recoil velocities acquired by fission isotopes coming from different fissioning systems. Surprisingly, the distribution of these systems extends over a rather wide range of elements: the most neutron-rich isotopes stem from the heaviest fissioning elements including uranium, while the neutron-deficient ones are populated by lighter fissioning systems like mercury. This trend is in agreement with the Z_{fiss}^2/A_{fiss}-dependence of the fissility: As a consequence of the low fissilities of light parent nuclei (low Z_{fiss}), only the most neutron-deficient isotopes (low A_{fiss}) have a chance for undergoing fission due to their smaller fission barriers; the residues produced by these parent nuclei
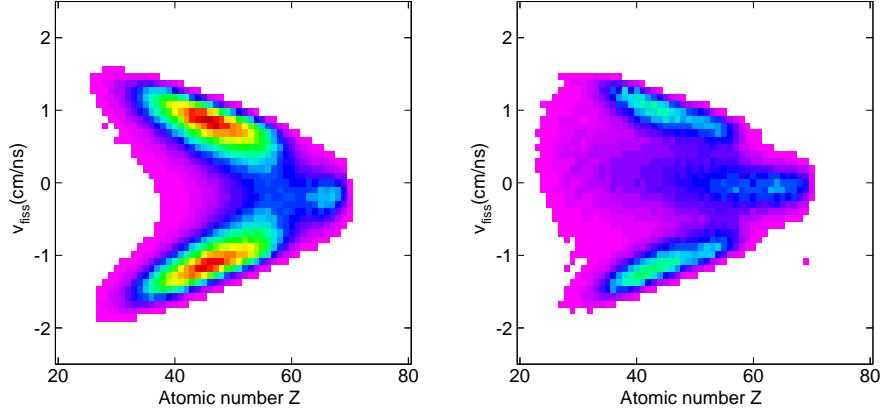
FIG. 9: Velocity distributions as a function of the atomic number of fragments measured with the deuterium target enclosed in the titanium container (left) and with the titanium dummy target (right).

populate thus the neutron-deficient side. On the contrary, the high fissilities of heavy fissioning systems are rather insensitive to a variation of the neutron number, thus extending their productions to more neutron-rich nuclei. A detailed analysis of these results will be discussed in a forthcoming paper.

B. Isotopic production cross-sections of fission fragments

The production cross-sections of 901 fission fragments measured in the present work are represented as a scatter-plot on the top of the chart of the nuclides in Fig. 13 (see also Tabs. IX-XVII). They cover a region on the neutron-rich side of the valley of stability, with elements ranging from vanadium to thulium. The most populated region corresponds to elements between niobium and cadmium with decreasing intensities for lower and higher atomic numbers. For most of these elements, the maximum productions span an extended flat ridge with 2-3 mass units on the right side of the valley of stability. Above the doubly closed shell Z=50 N=82, an enhanced fission fragment production is observed on the neutron-rich side.

Figures 14-16 provide a more detailed survey of the fission fragment production, showing the isotopic production cross sections for all measured fission fragments. The measured cross sections range from about 30 mb for intermediate masses of the different elements, down to values as low as 2 nb on the neutron-rich side.

As a general trend, the isotopic chains of the fission fragments follow a wide Gaussian distribution with mean neutron numbers slightly shifted toward the neutron-rich side of the valley of stability. The maximum production covers an extended region of elements around $_{46}$Pd, which corresponds to symmetric fission. For some elements above Z=50, these Gaussian shapes display a

pronounced shoulder in the neutron-rich side produced by the strong shell-effects around the double closed shell Z=50, N=126. The polarization of the heavy asymmetric fission fragments toward the neutron-rich side, makes the lighter asymmetric partners to move toward the valley of stability, leading to a less pronounced shoulder near the maximum of the isotopic chains, as shown for elements between $_{33}$As and $_{42}$Mo. This double-humped structure is not observed for elements above $_{59}$Pr and below $_{30}$Zn.

The total fission cross-section, obtained by summing up all the individual isotopic production cross-sections was found to be 2.00±0.42 barn. At the present moment, fission data of uranium on deuterium are scarcely represented in the current available databases. After a systematic literature search on the EXFOR [46] database, the only measurements found corresponded to deuteron-induced fission of uranium at energies below 200 MeV [47]. A comparison of these data with our results was possible by extrapolating the former according to the systematics of Prokofiev [48] for proton-induced fission reactions. In doing so, we had to consider the two main differences between proton and deuteron reactions at these energies, namely the average double energy introduced by deuterons, due to their additional nucleon, and the higher total reaction cross-section with respect to protons. Thus, the total fission cross-section measured by Stevenson et al. [47] at 190 MeV for deuteron-induced reactions on uranium (2.49±0.05 barn) was compared to the value given by Prokofiev at 2×190 MeV=380 MeV for protons (1.44 barn). The differences between these data were entirely attributed to the higher total reaction cross-section for deuterium, leading to a scaling factor of $S = 2.49/1.44 = 1.73$. In order to extrapolate the value of Stevenson measured at 190 MeV to 1 GeV, we multiplied the cross-section calculated by Prokofiev at 2 GeV (1.18 barn) by the factor S, which yields 2.04 barn. This value compares very well with our result.

The total reaction cross-sections could also be de-
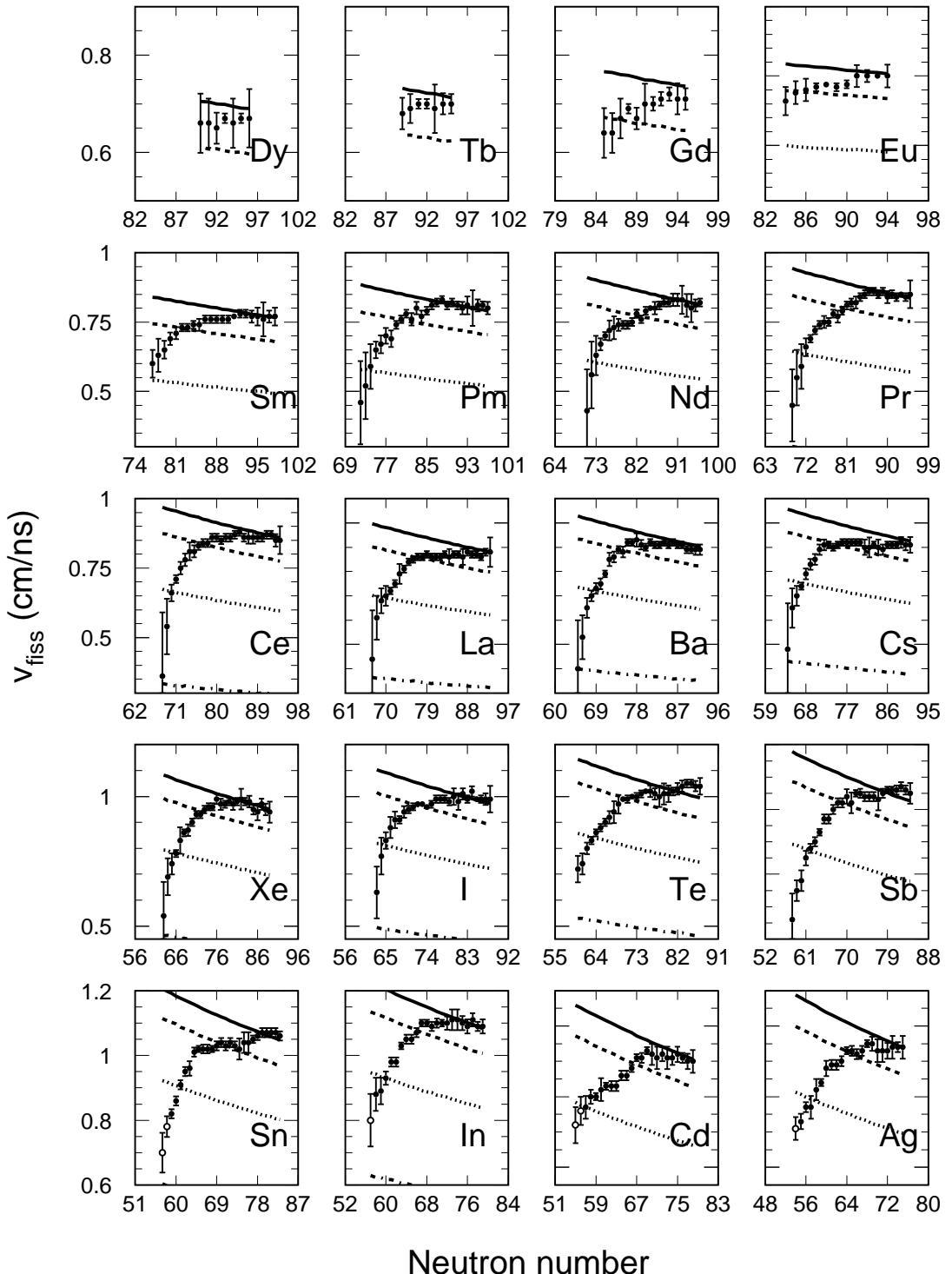
FIG. 10: Isotopic dependence of recoil velocities of fission fragments produced in ^{238}U(1A GeV)+d (dots) compared to the values calculated with the scission-model [45] (see text for details). The calculations were obtained for different fissioning systems: uranium Z=92 (solid line), radium Z=88 (dashed line), mercury Z=80 (dotted line) and rhenium Z=75 (dash-dotted line). Empty dots correspond to nuclei with a secondary-reaction contamination greater than 50%.
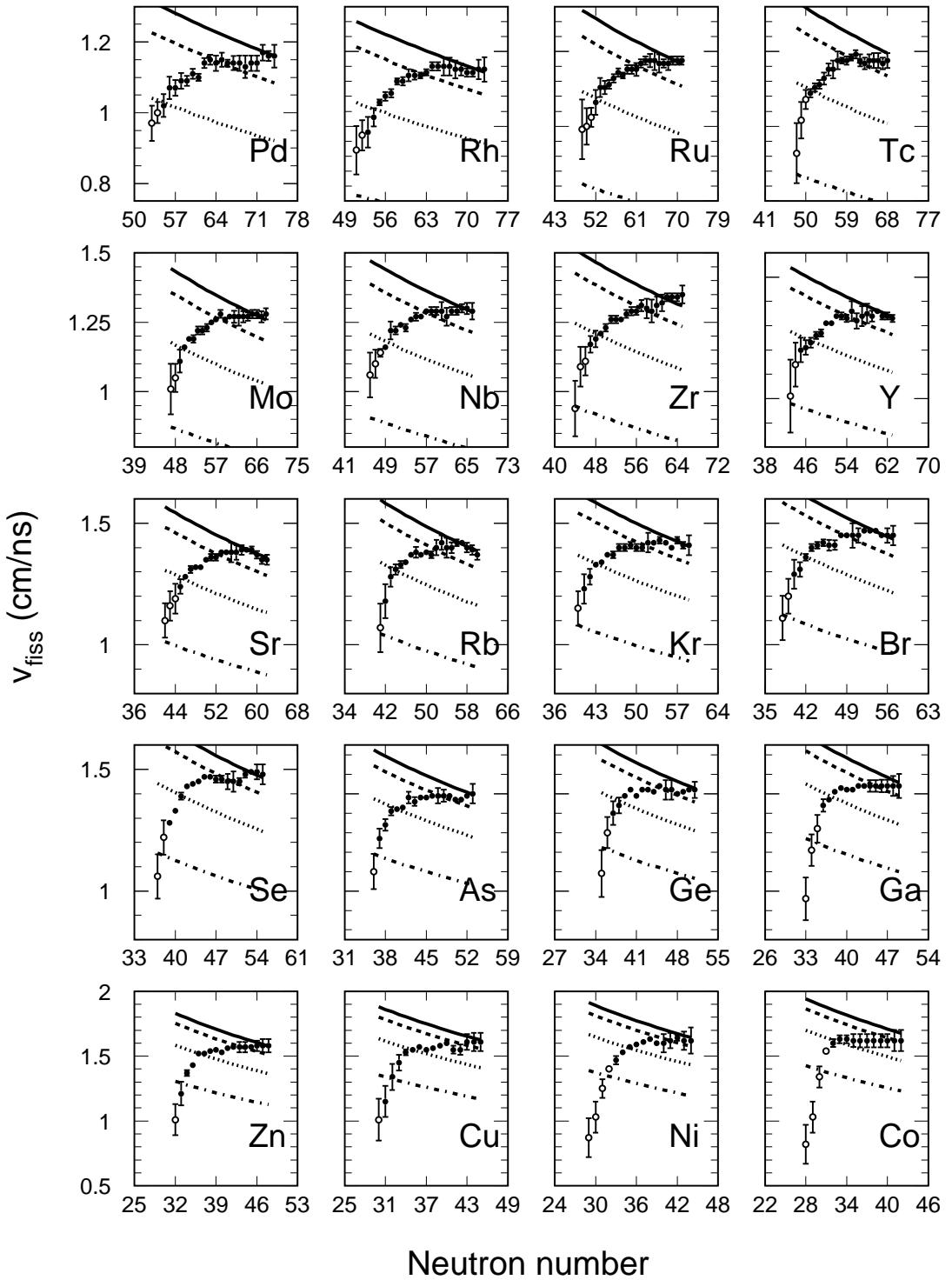
FIG. 11: Isotopic dependence of recoil velocities of fission fragments produced in ^{238}U(1A GeV)+d (dots) compared to the values calculated with the scission-model [45] (see text for details). The calculations were obtained for different fissioning systems: uranium Z=92 (solid line), radium Z=88 (dashed line), mercury Z=80 (dotted line) and rhenium Z=75 (dash-dotted line). Empty dots correspond to nuclei with a secondary-reaction contamination greater than 50%.
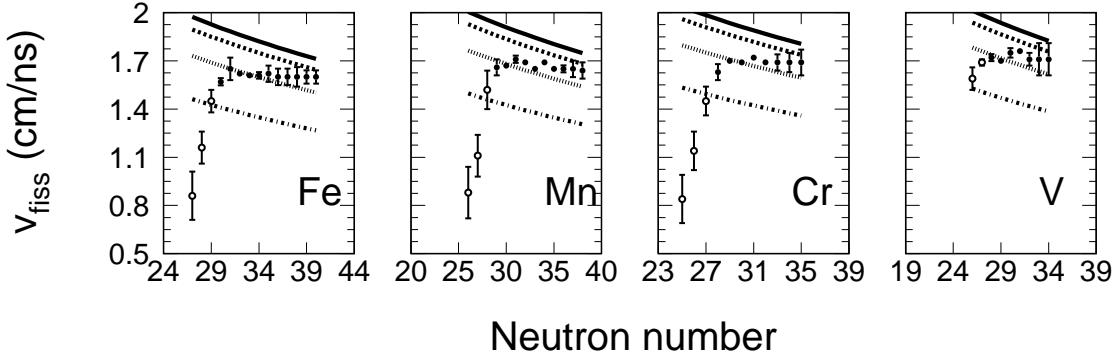
FIG. 12: Isotopic dependence of recoil velocities of fission fragments produced in ^{238}U(1A GeV)+d (dots) compared to the values calculated with the scission-model [45] (see text for details). The calculations were obtained for different fissioning systems: uranium Z=92 (solid line), radium Z=88 (dashed line), mercury Z=80 (dotted line) and rhenium Z=75 (dash-dotted line). Empty dots correspond to nuclei with a secondary-reaction contamination greater than 50%.
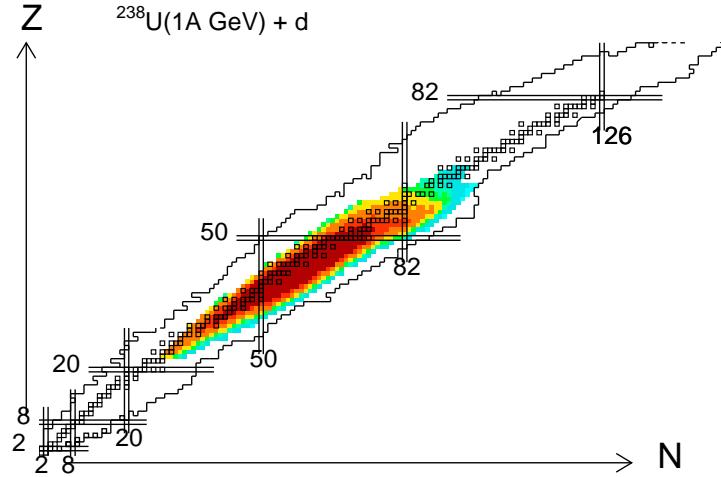
FIG. 13: Fission fragments in the reaction ^{238}U + d at 1A GeV on top of the chart of the nuclides. The grey scale indicates different production cross-sections.

termined by adding the total evaporation cross-section of 0.70±0.13 barn, obtained by E. Casarejos [11] for the reaction ^{238}U(1A GeV)+d to the total fission cross-section measured in the present work. The resulting value of 2.70±0.55 barn, is compatible with that of 2.51 barn calculated with the Glauber-type model of P.J. Karol [37], which assumes a Gaussian density profile with r(rms)=2.1fm for the deuteron nuclei [49]

In contrast to other existing experimental techniques, the total fission cross section obtained in the present work was not a directly measured observable, but deduced by summing up the contributions from every fission fragment. The isotopic production cross-sections of the fission fragments shown in Figs. 14-16 were obtained by applying different systematic corrections to the measured yields. Some of these corrections, like the angular transmission or the secondary reactions in the target, vary considerably as a function of the atomic and mass num-

bers of the final nuclei, reaching very large values in some cases. Any uncertainty in the determination of these corrections affected the values of the isotopic cross-sections, and consequently the value of the total cross-section. The high level of agreement between the total fission cross-section obtained in the present work and that deduced by extrapolation of a directly measured value [47] validates the methods used to determine these corrections. Similar conclusions are found when comparing the measured total reaction cross-section with the calculated value of Karol's model.
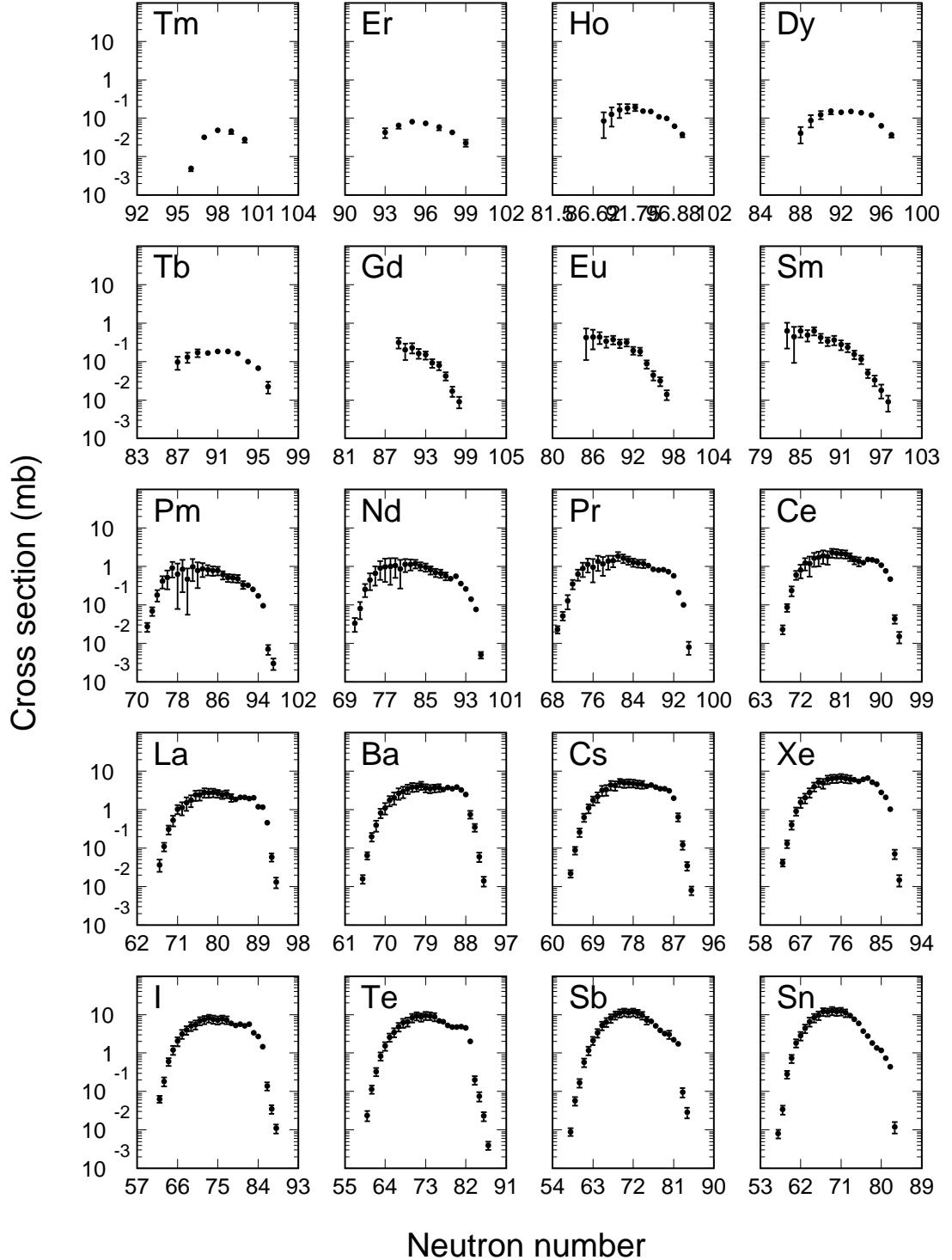
FIG. 14: Measured isotopic production cross-sections of fission fragments produced in the reaction ^{238}U(1A GeV)+d.
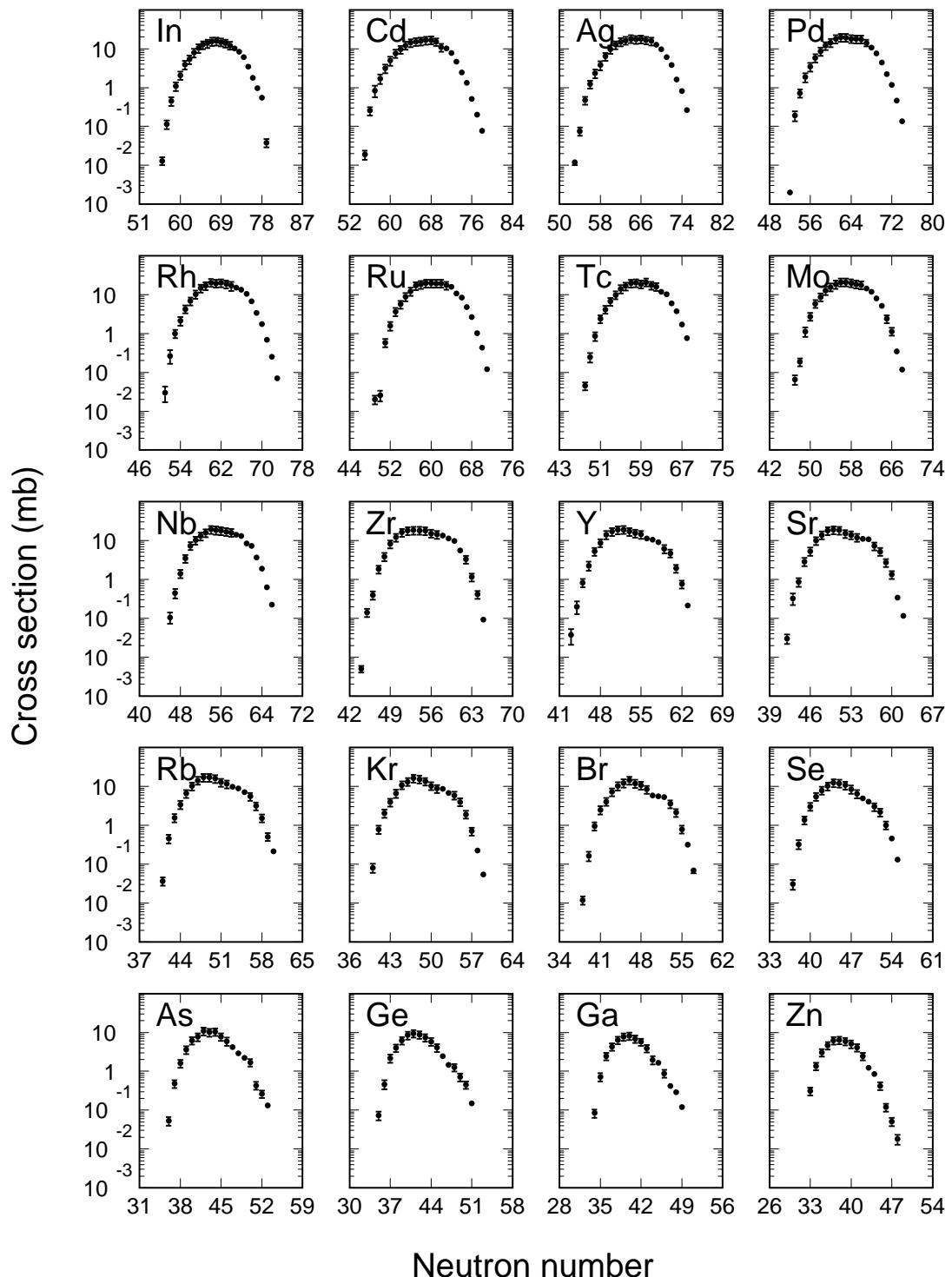
FIG. 15: Measured isotopic production cross-sections of fission fragments produced in the reaction ^{238}U(1A GeV)+d.
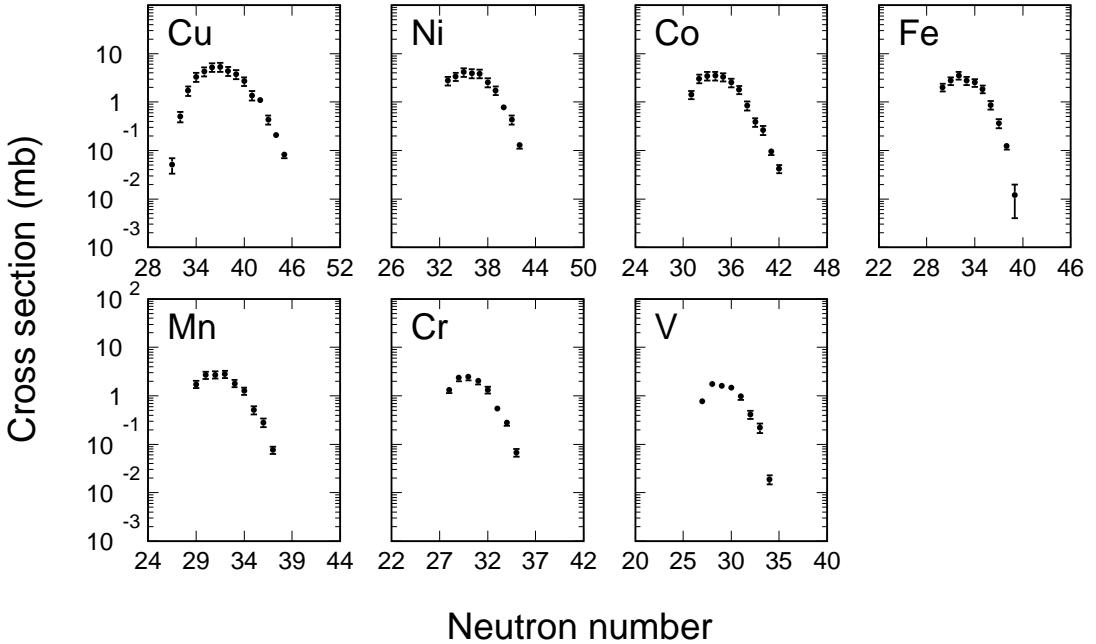
FIG. 16: Measured isotopic production cross-sections of fission fragments produced in the reaction ^{238}U(1A GeV)+d.

V. OUTLOOK

In the present work, the spallation-fission fragments produced in the reaction ^{238}U(1A GeV) on deuterium were experimentally investigated. The results obtained from the analysis include the evaluation of the recoil velocities and isotopic production cross-sections of 901 fission nuclei, which, together with the 602 evaporation fragments measured recently [11], constitutes one of the most extensive inventories of spallation-reaction productions ever measured before. The elements included in both experiments spread out over an extend region in the chart of nuclides, ranging from vanadium to thulium for the fission case, and from cerium to uranium for evaporation.

The precisions required for the present measurements were only attainable with the heavy-ion experimental facility at GSI (Germany). The uranium beam, accelerated in the Synchrotron accelerator SIS up to 1A GeV, was focused onto a cryogenic deuterium target placed at the entrance of the Fragment Separator (FRS), so that the forward-emitted fission fragments were transmitted through the separator. The optimum performance of the FRS, with a momentum resolving power of 1500, allowed the challenging separation of the reaction products, as well as their unambiguous identification according to the atomic and mass numbers.

The velocity distributions of the fission fragments were measured with relative resolutions of the order of 10^{-4}.

Fits to these velocity distributions allowed to separate the kinematics from evaporation and fission components. The results from the fits were introduced in an algorithm to extract the recoil velocities of the fission fragment. The precisions attained with this technique ranged typically from 1% to 5%, reaching maximum values of 20% in cases of very poor statistics or high contamination from evaporation reactions. Within a given element, the isotopic dependence of the fission velocities revealed a contribution from many different fissioning systems to the total productions. Moreover, the relatively low recoil velocities of some neutron deficient isotopes was found to be a sign of the contamination from multiple reactions induced by primary fission fragments.

The isotopic production cross-sections of the fission fragments were measured above the lower limit of 2 nb, with statistical uncertainties ranging from 1% to 5% for the majority of the measured fragments. The systematic error induced by the different corrections applied to the measured isotopic productions covers a wide range which extends from 10-20%, for most of the nuclei, to maximum values of 50% for very few cases. The main source of systematic error were the corrections that accounted for the multiple reactions in the production target and for the contamination from evaporation reactions. The maximum value of the cross-sections −around 30 mb− were found for intermediate-mass fragments around palladium-group elements. The isotopic chains of most of the fission fragments are well described by a

Gaussian function with mean neutron numbers slightly shifted towards the neutron-rich side of the valley of stability. For some elements above $Z=50$, a secondary maximum shows up in the neutron rich isotopes, revealing the high binding energies of nuclei around the double closed shell $Z=50$, $N=126$. When summing up the measured isotopic cross-sections, a total value of 2.00 ± 0.42 b was found, which is in good agreement with results obtained from Glauber-type models and extrapolations from experimental values. The addition of this cross-section to the value of 747 mb for the evaporation component [11], yields a total value of 2.747 b, which is in good agreement with Glauber-type calculations [37].

The richness of the present results demands a detailed discussion of the many different physical aspects underlying the investigated reaction.

Acknowledgments

APPENDIX A: RECOIL VELOCITY AND ISOTOPIC PRODUCTION CROSS-SECTIONS OF FISSION FRAGMENTS

[1] RNB VI Nucl. Phys. A748 (2005)
[2] The European Spallation Source Study, The ESS Technical Study, Vol. III, Report ESS-96-53-M, 1996
[3] C.D. Bowman, E.D. Arthur, P.W. Lisowski, G.P. Lawrence, R.J. Jensen, J.L. Anderson, B. Blind, M. Cappiello, J.W. Davidson, T.R. England, L.N. Engel, R.C. Gaight, H.G. Hughes, J.R. Ireland, R.A. Krakowski, R.J. LaBauve, B.C. Letellier, R.T. Perry, G.J. Russel, K.P. Staudhammer, G. Versamis and W.B. Wilson, Nucl. Instr. and Meth. A320 (1992) 336
[4] W.F. Henning, Nucl. Instr. and Meth. B126 (1997) 1
[5] R. Michel, I. Leya and L. Borges, Nucl. Instr. and Meth. B113 (1996) 343
[6] J. Pereira, Ph.D. Thesis, Universidade de Santiago de Compostela (2004)
[7] J. Benlliure, P. Armbruster, M. Bernas, A. Boudard, T. Enqvist, R. Legrain, S. Leray, F. Rejmund, K.-H. Schmidt, C. Stéphan, L. Tassan-Got and C. Volant, Nucl. Phys. A700 (2002) 469
[8] P. Napolitani, K.-H. Schmidt, A.S. Botvina, F. Rejmund, L. Tassan-Got and C. Villagrasa, accepted to be published in Phys. Rev. C
[9] K.-H. Schmidt, M.V. Ricciardi, A. Botvina and T. Enqvist, Nucl. Phys. A710 (2002) 157
[10] A.R. Junghans, M. de Jong, H.-G. Clerc, A.V. Ignatyuk, G.A. Kudyaev and K.-H. Schmidt, Nucl. Phys. A629 (1998) 635
[11] E. Casarejos, J. Benlliure, J. Pereira, P. Armbruster, M. Bernas, A. Boudard, S. Czajkowski, T. Enqvist, R. Legrain, S. Leray, B. Mustapha, M. Pravikoff, F. Rejmund, K.-H. Schmidt, C. Stephan, J. Taíeb, L. Tassan-Got, C. Volant and W. Wlazlo, submitted to Phys. Rev. C
[12] W. Wlazlo, T. Enqvist, P. Armbruster, J. Benlliure, M. Bernas, A. Boudard, C. Czajkowski, R. Legrain, S. Leray, B. Mustapha, M. Pravikoff, F. Rejmund, K.-H. Schmidt, C. Stéphan, J. Taïeb, L. Tassan-Got and C. Volant, Phys. Rev. Lett. 84 (2000) 5736
[13] J. Benlliure, P. Armbruster, M. Bernas, A. Boudard, J.P. Dufour, T. Enqvist, R. Legrain, S. Leray, B. Mustapha, F. Rejmund, K.-H. Schmidt, C. Stéphan, L. Tassan-Got and C. Volant Nucl. Phys. A683 (2001) 513
[14] F. Rejmund, B. Mustapha, P. Armbruster, J. Benlliure, M. Bernas, A. Boudard, J.P. Dufour, T. Enqvist, R. Legrain, S. Leray, M. Pravikoff, F. Rejmund, K.-H. Schmidt, C. Stéphan, J. Taïeb, L. Tassan-Got, C. Volant and W. Wlazlo, Nucl. Phys. A 683 (2001) 540
[15] T. Enqvist, W. Wlazlo, P. Armbruster, J. Benlliure, M. Bernas, A. Boudard, S. Czajkowski, R. Legrain, S. Leray, B. Mustapha, M. Pravikoff, F. Rejmund, K.-H. Schmidt, C. Stéphan, J. Taíeb, L. Tassan-Got and C. Volant Nucl. Phys. A 686 (2001) 481
[16] T. Enqvist, P. Armbruster, J. Benlliure, M. Bernas, A. Boudard, S. Czajkowski, R. Legrain, S. Leray, B. Mustapha, M. Pravikoff, F. Rejmund, K.-H. Schmidt, C. Stéphan, J. Taíeb, L. Tassan-Got, F. Vivès, C. Volant and W. Wlazlo, Nucl. Phys. A 703 (2002) 435
[17] J. Taïeb, K.-H. Schmidt, L. Tassan-Got, P. Armbruster, J. Benlliure, M. Bernas, A. Boudard, E. Casarejos, S. Czajkowski, T. Enqvist, R. Legrain, S. Leray, B. Mustapha, M. Pravikoff, F. Rejmund, C. Stephan, C. Volant and W. Wlazlo, Nucl. Phys. A724 (2003) 213
[18] M. Bernas, P. Armbruster, J. Benlliure, A. Boudard, E. Casarejos, S. Czajkowski, T. Enqvist, R. Legrain, S. Leray, B. Mustapha, P. Napolitani, J. Pereira, F. Rejmund, M. V. Ricciardi, K.-H. Schmidt, C. Stéphan, J. Taíeb, L. Tassan-Got, C. Volant and W. Wlazlo, Nucl. Phys. A725 (2003) 213
[19] P. Armbruster, J. Benlliure, M. Bernas, A. Boudard,

nucleus	v_{fiss} (cm/ns)	ε_{tot} (cm/ns)	nucleus	v_{fiss} (cm/ns)	ε_{tot} (cm/ns)
^{49}V	1.590	0.070	^{65}Co	1.620	0.051
^{50}V	1.690	0.020	^{66}Co	1.620	0.051
^{51}V	1.720	0.022	^{67}Co	1.620	0.051
^{52}V	1.700	0.010	^{68}Co	1.620	0.081
^{53}V	1.750	0.030	^{69}Co	1.620	0.081
^{54}V	1.760	0.010	^{57}Ni	0.870	0.150
^{55}V	1.710	0.040	^{58}Ni	1.030	0.120
^{56}V	1.710	0.100	^{59}Ni	1.250	0.071
^{57}V	1.710	0.100	^{60}Ni	1.400	0.020
^{49}Cr	0.840	0.150	^{61}Ni	1.470	0.032
^{50}Cr	1.140	0.120	^{62}Ni	1.530	0.010
^{51}Cr	1.450	0.090	^{63}Ni	1.570	0.014
^{52}Cr	1.630	0.050	^{64}Ni	1.590	0.010
^{53}Cr	1.700	0.010	^{65}Ni	1.610	0.010
^{54}Cr	1.690	0.010	^{66}Ni	1.630	0.010
^{55}Cr	1.720	0.010	^{67}Ni	1.600	0.014
^{56}Cr	1.690	0.010	^{68}Ni	1.600	0.071
^{57}Cr	1.690	0.050	^{69}Ni	1.620	0.060
^{58}Cr	1.690	0.060	^{70}Ni	1.640	0.022
^{59}Cr	1.690	0.080	^{71}Ni	1.620	0.070
^{51}Mn	0.880	0.160	^{72}Ni	1.620	0.100
^{52}Mn	1.110	0.130	^{59}Cu	1.010	0.160
^{53}Mn	1.520	0.120	^{60}Cu	1.150	0.120
^{54}Mn	1.660	0.050	^{61}Cu	1.340	0.100
^{55}Mn	1.670	0.010	^{62}Cu	1.450	0.061
^{56}Mn	1.710	0.022	^{63}Cu	1.530	0.022
^{57}Mn	1.690	0.014	^{64}Cu	1.550	0.014
^{58}Mn	1.650	0.010	^{65}Cu	1.570	0.014
^{59}Mn	1.690	0.010	^{66}Cu	1.550	0.014
^{60}Mn	1.650	0.014	^{67}Cu	1.560	0.010
^{61}Mn	1.650	0.022	^{68}Cu	1.580	0.014
^{62}Mn	1.650	0.051	^{69}Cu	1.600	0.010
^{63}Mn	1.640	0.051	^{70}Cu	1.550	0.030
^{53}Fe	0.860	0.150	^{71}Cu	1.550	0.040
^{54}Fe	1.160	0.100	^{72}Cu	1.610	0.060
^{55}Fe	1.450	0.070	^{73}Cu	1.610	0.070
^{56}Fe	1.570	0.022	^{74}Cu	1.610	0.071
^{57}Fe	1.650	0.070	^{62}Zn	1.010	0.120
^{58}Fe	1.620	0.010	^{63}Zn	1.210	0.091
^{59}Fe	1.610	0.010	^{64}Zn	1.370	0.022
^{60}Fe	1.610	0.020	^{65}Zn	1.430	0.014
^{61}Fe	1.620	0.050	^{66}Zn	1.520	0.010
^{62}Fe	1.600	0.051	^{67}Zn	1.520	0.014
^{63}Fe	1.600	0.051	^{68}Zn	1.540	0.010
^{64}Fe	1.600	0.061	^{69}Zn	1.550	0.010
^{65}Fe	1.600	0.041	^{70}Zn	1.530	0.010
^{66}Fe	1.600	0.041	^{71}Zn	1.560	0.010
^{55}Co	0.820	0.150	^{72}Zn	1.570	0.020
^{56}Co	1.030	0.120	^{73}Zn	1.570	0.040
^{57}Co	1.340	0.081	^{74}Zn	1.570	0.040
^{58}Co	1.540	0.010	^{75}Zn	1.570	0.014
^{59}Co	1.600	0.030	^{76}Zn	1.580	0.040
^{60}Co	1.630	0.030	^{77}Zn	1.580	0.050
^{61}Co	1.630	0.030	^{78}Zn	1.580	0.050
^{62}Co	1.620	0.050	^{64}Ga	0.960	0.110
^{63}Co	1.620	0.051	^{65}Ga	1.210	0.081
^{64}Co	1.620	0.051	^{66}Ga	1.320	0.071

TABLE I: Recoil velocities of fission fragments (in cm/ns) measured in the frame of the fissioning system for the reaction ^{238}U(1A GeV)+d, with their total error.

nucleus	v_{fiss} (cm/ns)	ε_{tot} (cm/ns)	nucleus	v_{fiss} (cm/ns)	ε_{tot} (cm/ns)
^{67}Ga	1.440	0.032	^{79}Se	1.470	0.010
^{68}Ga	1.470	0.010	^{80}Se	1.470	0.010
^{69}Ga	1.510	0.010	^{81}Se	1.460	0.014
^{70}Ga	1.530	0.014	^{82}Se	1.460	0.014
^{71}Ga	1.520	0.014	^{83}Se	1.450	0.032
^{72}Ga	1.520	0.014	^{84}Se	1.450	0.041
^{73}Ga	1.540	0.014	^{85}Se	1.450	0.014
^{74}Ga	1.540	0.014	^{86}Se	1.480	0.014
^{75}Ga	1.540	0.030	^{87}Se	1.490	0.010
^{76}Ga	1.540	0.030	^{88}Se	1.490	0.030
^{77}Ga	1.540	0.032	^{89}Se	1.480	0.041
^{78}Ga	1.540	0.032	^{73}Br	1.110	0.091
^{79}Ga	1.540	0.051	^{74}Br	1.200	0.071
^{80}Ga	1.540	0.061	^{75}Br	1.290	0.060
^{67}Ge	1.090	0.120	^{76}Br	1.310	0.030
^{68}Ge	1.300	0.080	^{77}Br	1.360	0.014
^{69}Ge	1.400	0.061	^{78}Br	1.400	0.014
^{70}Ge	1.440	0.040	^{79}Br	1.410	0.014
^{71}Ge	1.490	0.010	^{80}Br	1.420	0.014
^{72}Ge	1.520	0.010	^{81}Br	1.410	0.022
^{73}Ge	1.490	0.014	^{82}Br	1.410	0.020
^{74}Ge	1.520	0.014	^{83}Br	1.450	0.010
^{75}Ge	1.520	0.014	^{84}Br	1.450	0.010
^{76}Ge	1.510	0.010	^{85}Br	1.450	0.050
^{77}Ge	1.540	0.010	^{86}Br	1.450	0.030
^{78}Ge	1.520	0.050	^{87}Br	1.470	0.010
^{79}Ge	1.520	0.050	^{88}Br	1.470	0.010
^{80}Ge	1.500	0.014	^{89}Br	1.470	0.010
^{81}Ge	1.510	0.014	^{90}Br	1.450	0.010
^{82}Ge	1.520	0.014	^{91}Br	1.450	0.030
^{83}Ge	1.520	0.041	^{92}Br	1.450	0.040
^{69}As	1.100	0.090	^{76}Kr	1.150	0.071
^{70}As	1.270	0.050	^{77}Kr	1.230	0.061
^{71}As	1.340	0.030	^{78}Kr	1.280	0.032
^{72}As	1.410	0.022	^{79}Kr	1.330	0.010
^{73}As	1.420	0.014	^{80}Kr	1.340	0.010
^{74}As	1.430	0.014	^{81}Kr	1.370	0.010
^{75}As	1.480	0.030	^{82}Kr	1.370	0.014
^{76}As	1.460	0.022	^{83}Kr	1.400	0.014
^{77}As	1.480	0.010	^{84}Kr	1.400	0.014
^{78}As	1.480	0.010	^{85}Kr	1.410	0.014
^{79}As	1.490	0.010	^{86}Kr	1.400	0.014
^{80}As	1.490	0.040	^{87}Kr	1.400	0.014
^{81}As	1.490	0.030	^{88}Kr	1.420	0.040
^{82}As	1.490	0.010	^{89}Kr	1.420	0.010
^{83}As	1.470	0.010	^{90}Kr	1.430	0.014
^{84}As	1.470	0.010	^{91}Kr	1.420	0.010
^{85}As	1.490	0.014	^{92}Kr	1.400	0.010
^{86}As	1.500	0.050	^{93}Kr	1.430	0.014
^{71}Se	1.060	0.091	^{94}Kr	1.410	0.014
^{72}Se	1.220	0.071	^{95}Kr	1.410	0.041
^{73}Se	1.280	0.010	^{78}Rb	1.070	0.100
^{74}Se	1.330	0.010	^{79}Rb	1.180	0.070
^{75}Se	1.390	0.014	^{80}Rb	1.280	0.040
^{76}Se	1.430	0.010	^{81}Rb	1.310	0.022
^{77}Se	1.440	0.010	^{82}Rb	1.330	0.014
^{78}Se	1.450	0.010	^{83}Rb	1.340	0.010

TABLE II: Recoil velocities of fission fragments (in cm/ns) measured in the frame of the fissioning system for the reaction ^{238}U(1A GeV)+d, with their total error.

nucleus	v_{fiss} (cm/ns)	ε_{tot} (cm/ns)	nucleus	v_{fiss} (cm/ns)	ε_{tot} (cm/ns)
^{84}Rb	1.370	0.010	^{85}Zr	1.090	0.071
^{85}Rb	1.380	0.022	^{86}Zr	1.110	0.051
^{86}Rb	1.370	0.010	^{87}Zr	1.170	0.030
^{87}Rb	1.380	0.010	^{88}Zr	1.190	0.030
^{88}Rb	1.370	0.014	^{89}Zr	1.210	0.010
^{89}Rb	1.400	0.032	^{90}Zr	1.230	0.014
^{90}Rb	1.420	0.030	^{91}Zr	1.260	0.014
^{91}Rb	1.400	0.041	^{92}Zr	1.260	0.014
^{92}Rb	1.400	0.022	^{93}Zr	1.260	0.010
^{93}Rb	1.420	0.014	^{94}Zr	1.280	0.014
^{94}Rb	1.420	0.010	^{95}Zr	1.290	0.015
^{95}Rb	1.400	0.020	^{96}Zr	1.290	0.014
^{96}Rb	1.390	0.020	^{97}Zr	1.310	0.020
^{97}Rb	1.370	0.020	^{98}Zr	1.300	0.035
^{80}Sr	1.100	0.071	^{99}Zr	1.290	0.041
^{81}Sr	1.160	0.061	^{100}Zr	1.310	0.032
^{82}Sr	1.190	0.061	^{101}Zr	1.320	0.030
^{83}Sr	1.240	0.030	^{102}Zr	1.340	0.014
^{84}Sr	1.280	0.010	^{103}Zr	1.340	0.014
^{85}Sr	1.310	0.014	^{104}Zr	1.340	0.014
^{86}Sr	1.320	0.010	^{105}Zr	1.350	0.032
^{87}Sr	1.320	0.010	^{87}Nb	1.060	0.080
^{88}Sr	1.350	0.010	^{88}Nb	1.100	0.051
^{89}Sr	1.360	0.014	^{89}Nb	1.140	0.014
^{90}Sr	1.360	0.014	^{90}Nb	1.160	0.010
^{91}Sr	1.380	0.010	^{91}Nb	1.220	0.032
^{92}Sr	1.380	0.010	^{92}Nb	1.220	0.014
^{93}Sr	1.380	0.040	^{93}Nb	1.240	0.010
^{94}Sr	1.380	0.030	^{94}Nb	1.230	0.014
^{95}Sr	1.390	0.020	^{95}Nb	1.260	0.010
^{96}Sr	1.390	0.010	^{96}Nb	1.270	0.014
^{97}Sr	1.390	0.014	^{97}Nb	1.270	0.010
^{98}Sr	1.370	0.015	^{98}Nb	1.290	0.010
^{99}Sr	1.350	0.017	^{99}Nb	1.290	0.014
^{100}Sr	1.350	0.020	^{100}Nb	1.290	0.014
^{82}Y	1.010	0.150	^{101}Nb	1.290	0.032
^{83}Y	1.140	0.091	^{102}Nb	1.270	0.032
^{84}Y	1.200	0.050	^{103}Nb	1.290	0.014
^{85}Y	1.210	0.030	^{104}Nb	1.290	0.014
^{86}Y	1.230	0.020	^{105}Nb	1.300	0.015
^{87}Y	1.260	0.014	^{106}Nb	1.300	0.020
^{88}Y	1.270	0.014	^{107}Nb	1.290	0.030
^{89}Y	1.310	0.010	^{89}Mo	1.010	0.091
^{90}Y	1.310	0.010	^{90}Mo	1.050	0.051
^{91}Y	1.340	0.010	^{91}Mo	1.110	0.041
^{92}Y	1.340	0.014	^{92}Mo	1.160	0.010
^{93}Y	1.330	0.014	^{93}Mo	1.190	0.010
^{94}Y	1.360	0.041	^{94}Mo	1.190	0.014
^{95}Y	1.320	0.032	^{95}Mo	1.220	0.014
^{96}Y	1.340	0.041	^{96}Mo	1.220	0.014
^{97}Y	1.350	0.040	^{97}Mo	1.230	0.014
^{98}Y	1.340	0.022	^{98}Mo	1.250	0.010
^{99}Y	1.360	0.010	^{99}Mo	1.260	0.010
^{100}Y	1.340	0.015	^{100}Mo	1.280	0.014
^{101}Y	1.340	0.015	^{101}Mo	1.260	0.010
^{102}Y	1.330	0.015	^{102}Mo	1.270	0.010
^{84}Zr	0.940	0.100	^{103}Mo	1.270	0.022

nucleus	v_{fiss} (cm/ns)	ε_{tot} (cm/ns)	nucleus	v_{fiss} (cm/ns)	ε_{tot} (cm/ns)
^{104}Mo	1.270	0.032	^{102}Rh	1.110	0.014
^{105}Mo	1.270	0.020	^{103}Rh	1.150	0.010
^{106}Mo	1.270	0.015	^{104}Rh	1.150	0.014
^{107}Mo	1.280	0.015	^{105}Rh	1.170	0.020
^{108}Mo	1.280	0.015	^{106}Rh	1.170	0.014
^{109}Mo	1.270	0.020	^{107}Rh	1.170	0.010
^{110}Mo	1.280	0.020	^{108}Rh	1.180	0.010
^{91}Tc	0.910	0.100	^{109}Rh	1.200	0.014
^{92}Tc	1.020	0.061	^{110}Rh	1.200	0.014
^{93}Tc	1.090	0.032	^{111}Rh	1.200	0.030
^{94}Tc	1.110	0.014	^{112}Rh	1.200	0.030
^{95}Tc	1.130	0.014	^{113}Rh	1.190	0.030
^{96}Tc	1.140	0.014	^{114}Rh	1.190	0.020
^{97}Tc	1.160	0.020	^{115}Rh	1.180	0.014
^{98}Tc	1.190	0.020	^{116}Rh	1.180	0.014
^{99}Tc	1.190	0.030	^{117}Rh	1.190	0.032
^{100}Tc	1.220	0.030	^{118}Rh	1.190	0.041
^{101}Tc	1.220	0.010	^{99}Pd	0.970	0.050
^{102}Tc	1.220	0.014	^{100}Pd	1.000	0.030
^{103}Tc	1.230	0.010	^{101}Pd	1.020	0.032
^{104}Tc	1.240	0.014	^{102}Pd	1.070	0.032
^{105}Tc	1.220	0.020	^{103}Pd	1.070	0.022
^{106}Tc	1.210	0.020	^{104}Pd	1.090	0.022
^{107}Tc	1.220	0.020	^{105}Pd	1.090	0.014
^{108}Tc	1.220	0.025	^{106}Pd	1.110	0.014
^{109}Tc	1.220	0.025	^{107}Pd	1.100	0.010
^{110}Tc	1.210	0.020	^{108}Pd	1.140	0.014
^{111}Tc	1.220	0.025	^{109}Pd	1.150	0.014
^{93}Ru	0.990	0.100	^{110}Pd	1.140	0.022
^{94}Ru	1.000	0.061	^{111}Pd	1.150	0.020
^{95}Ru	1.030	0.032	^{112}Pd	1.140	0.010
^{96}Ru	1.080	0.041	^{113}Pd	1.140	0.020
^{97}Ru	1.130	0.032	^{114}Pd	1.140	0.022
^{98}Ru	1.130	0.022	^{115}Pd	1.130	0.032
^{99}Ru	1.140	0.014	^{116}Pd	1.140	0.022
^{100}Ru	1.160	0.014	^{117}Pd	1.140	0.022
^{101}Ru	1.180	0.014	^{118}Pd	1.170	0.022
^{102}Ru	1.170	0.010	^{119}Pd	1.160	0.014
^{103}Ru	1.190	0.014	^{120}Pd	1.160	0.032
^{104}Ru	1.190	0.014	^{101}Ag	0.910	0.032
^{105}Ru	1.190	0.022	^{102}Ag	0.930	0.022
^{106}Ru	1.210	0.014	^{103}Ag	0.970	0.014
^{107}Ru	1.220	0.014	^{104}Ag	0.970	0.032
^{108}Ru	1.220	0.022	^{105}Ag	1.020	0.030
^{109}Ru	1.220	0.032	^{106}Ag	1.040	0.010
^{110}Ru	1.210	0.030	^{107}Ag	1.080	0.022
^{111}Ru	1.210	0.014	^{108}Ag	1.090	0.014
^{112}Ru	1.210	0.022	^{109}Ag	1.090	0.014
^{113}Ru	1.220	0.014	^{110}Ag	1.100	0.014
^{114}Ru	1.220	0.014	^{111}Ag	1.130	0.010
^{115}Ru	1.220	0.014	^{112}Ag	1.130	0.014
^{96}Rh	0.920	0.081	^{113}Ag	1.120	0.014
^{97}Rh	0.970	0.051	^{114}Ag	1.130	0.014
^{98}Rh	0.980	0.051	^{115}Ag	1.150	0.010
^{99}Rh	1.030	0.030	^{116}Ag	1.150	0.020
^{100}Rh	1.080	0.010	^{117}Ag	1.130	0.032
^{101}Rh	1.100	0.014	^{118}Ag	1.130	0.032

TABLE III: Recoil velocities of fission fragments (in cm/ns) measured in the frame of the fissioning system for the reaction ^{238}U(1A GeV)+d, with their total error.

TABLE IV: Recoil velocities of fission fragments (in cm/ns) measured in the frame of the fissioning system for the reaction ^{238}U(1A GeV)+d, with their total error.

nucleus	v_{fiss} (cm/ns)	ε_{tot} (cm/ns)	nucleus	v_{fiss} (cm/ns)	ε_{tot} (cm/ns)
^{119}Ag	1.130	0.022	^{113}Sn	0.960	0.022
^{120}Ag	1.140	0.032	^{114}Sn	1.010	0.014
^{121}Ag	1.140	0.014	^{115}Sn	1.020	0.010
^{122}Ag	1.140	0.032	^{116}Sn	1.020	0.014
^{103}Cd	0.920	0.051	^{117}Sn	1.020	0.014
^{104}Cd	0.960	0.040	^{118}Sn	1.020	0.010
^{105}Cd	0.970	0.032	^{119}Sn	1.030	0.014
^{106}Cd	1.000	0.020	^{120}Sn	1.040	0.014
^{107}Cd	1.000	0.010	^{121}Sn	1.030	0.014
^{108}Cd	1.020	0.032	^{122}Sn	1.040	0.014
^{109}Cd	1.030	0.010	^{123}Sn	1.030	0.014
^{110}Cd	1.030	0.014	^{124}Sn	1.020	0.032
^{111}Cd	1.030	0.014	^{125}Sn	1.040	0.032
^{112}Cd	1.060	0.014	^{126}Sn	1.040	0.032
^{113}Cd	1.060	0.014	^{127}Sn	1.050	0.012
^{114}Cd	1.080	0.010	^{128}Sn	1.060	0.012
^{115}Cd	1.110	0.010	^{129}Sn	1.070	0.014
^{116}Cd	1.110	0.014	^{130}Sn	1.070	0.014
^{117}Cd	1.130	0.010	^{131}Sn	1.070	0.014
^{118}Cd	1.120	0.030	^{132}Sn	1.070	0.014
^{119}Cd	1.110	0.032	^{133}Sn	1.060	0.014
^{120}Cd	1.120	0.020	^{109}Sb	0.660	0.081
^{121}Cd	1.110	0.032	^{110}Sb	0.750	0.032
^{122}Cd	1.110	0.020	^{111}Sb	0.780	0.032
^{123}Cd	1.120	0.022	^{112}Sb	0.850	0.022
^{124}Cd	1.110	0.014	^{113}Sb	0.880	0.014
^{125}Cd	1.100	0.022	^{114}Sb	0.900	0.014
^{126}Cd	1.100	0.032	^{115}Sb	0.930	0.010
^{106}In	0.800	0.081	^{116}Sb	0.970	0.014
^{107}In	0.880	0.051	^{117}Sb	0.970	0.014
^{108}In	0.890	0.041	^{118}Sb	1.000	0.014
^{109}In	0.930	0.020	^{119}Sb	1.020	0.014
^{110}In	0.980	0.014	^{120}Sb	1.020	0.014
^{111}In	0.980	0.014	^{121}Sb	1.040	0.022
^{112}In	1.030	0.010	^{122}Sb	1.020	0.032
^{113}In	1.050	0.014	^{123}Sb	1.050	0.010
^{114}In	1.050	0.014	^{124}Sb	1.050	0.014
^{115}In	1.070	0.014	^{125}Sb	1.040	0.014
^{116}In	1.100	0.010	^{126}Sb	1.040	0.014
^{117}In	1.100	0.010	^{127}Sb	1.040	0.014
^{118}In	1.090	0.014	^{128}Sb	1.030	0.032
^{119}In	1.100	0.014	^{129}Sb	1.050	0.014
^{120}In	1.100	0.010	^{130}Sb	1.060	0.010
^{121}In	1.100	0.020	^{131}Sb	1.060	0.010
^{122}In	1.110	0.032	^{132}Sb	1.060	0.014
^{123}In	1.110	0.032	^{133}Sb	1.070	0.014
^{124}In	1.100	0.022	^{134}Sb	1.060	0.014
^{125}In	1.090	0.022	^{135}Sb	1.050	0.032
^{126}In	1.110	0.020	^{112}Te	0.720	0.051
^{127}In	1.090	0.014	^{113}Te	0.740	0.041
^{128}In	1.090	0.022	^{114}Te	0.800	0.022
^{107}Sn	0.700	0.061	^{115}Te	0.830	0.014
^{108}Sn	0.780	0.032	^{116}Te	0.860	0.014
^{109}Sn	0.820	0.014	^{117}Te	0.880	0.014
^{110}Sn	0.860	0.014	^{118}Te	0.900	0.014
^{111}Sn	0.910	0.014	^{119}Te	0.920	0.024
^{112}Sn	0.950	0.014	^{120}Te	0.940	0.042

TABLE V: Recoil velocities of fission fragments (in cm/ns) measured in the frame of the fissioning system for the reaction ^{238}U(1A GeV)+d, with their total error.

nucleus	v_{fiss} (cm/ns)	ε_{tot} (cm/ns)	nucleus	v_{fiss} (cm/ns)	ε_{tot} (cm/ns)
^{121}Te	0.970	0.036	^{129}Xe	0.960	0.014
^{122}Te	0.990	0.010	^{130}Xe	0.990	0.020
^{123}Te	0.990	0.014	^{131}Xe	0.970	0.022
^{124}Te	1.000	0.010	^{132}Xe	0.970	0.014
^{125}Te	1.000	0.014	^{133}Xe	0.980	0.014
^{126}Te	1.010	0.014	^{134}Xe	0.970	0.022
^{127}Te	1.020	0.010	^{135}Xe	0.980	0.014
^{128}Te	1.020	0.022	^{136}Xe	0.990	0.040
^{129}Te	1.010	0.022	^{137}Xe	0.980	0.014
^{130}Te	1.000	0.041	^{138}Xe	0.980	0.022
^{131}Te	1.010	0.041	^{139}Xe	0.950	0.020
^{132}Te	1.010	0.032	^{140}Xe	0.940	0.032
^{133}Te	1.020	0.015	^{141}Xe	0.970	0.022
^{134}Te	1.030	0.022	^{142}Xe	0.950	0.022
^{135}Te	1.040	0.022	^{143}Xe	0.940	0.041
^{136}Te	1.050	0.015	^{119}Cs	0.480	0.190
^{137}Te	1.050	0.015	^{120}Cs	0.650	0.081
^{138}Te	1.040	0.020	^{121}Cs	0.700	0.041
^{139}Te	1.040	0.032	^{122}Cs	0.740	0.014
^{116}I	0.630	0.100	^{123}Cs	0.790	0.022
^{117}I	0.770	0.071	^{124}Cs	0.830	0.022
^{118}I	0.830	0.032	^{125}Cs	0.850	0.022
^{119}I	0.880	0.041	^{126}Cs	0.890	0.022
^{120}I	0.910	0.032	^{127}Cs	0.910	0.022
^{121}I	0.910	0.014	^{128}Cs	0.910	0.014
^{122}I	0.940	0.022	^{129}Cs	0.900	0.014
^{123}I	0.950	0.014	^{130}Cs	0.910	0.014
^{124}I	0.960	0.014	^{131}Cs	0.920	0.014
^{125}I	0.970	0.010	^{132}Cs	0.920	0.014
^{126}I	0.970	0.010	^{133}Cs	0.920	0.014
^{127}I	0.960	0.010	^{134}Cs	0.920	0.014
^{128}I	0.970	0.014	^{135}Cs	0.920	0.014
^{129}I	0.990	0.014	^{136}Cs	0.900	0.032
^{130}I	0.990	0.014	^{137}Cs	0.900	0.041
^{131}I	0.990	0.014	^{138}Cs	0.910	0.014
^{132}I	0.980	0.014	^{139}Cs	0.900	0.032
^{133}I	1.000	0.032	^{140}Cs	0.890	0.022
^{134}I	0.980	0.032	^{141}Cs	0.910	0.014
^{135}I	1.010	0.022	^{142}Cs	0.910	0.014
^{136}I	0.990	0.014	^{143}Cs	0.910	0.014
^{137}I	1.020	0.020	^{144}Cs	0.920	0.022
^{138}I	0.990	0.010	^{145}Cs	0.910	0.022
^{139}I	0.990	0.014	^{146}Cs	0.910	0.032
^{140}I	0.990	0.022	^{121}Ba	0.400	0.200
^{141}I	0.990	0.051	^{122}Ba	0.530	0.090
^{117}Xe	0.540	0.130	^{123}Ba	0.650	0.041
^{118}Xe	0.690	0.071	^{124}Ba	0.700	0.022
^{119}Xe	0.740	0.041	^{125}Ba	0.730	0.022
^{120}Xe	0.780	0.014	^{126}Ba	0.750	0.022
^{121}Xe	0.830	0.051	^{127}Ba	0.790	0.014
^{122}Xe	0.860	0.014	^{128}Ba	0.850	0.028
^{123}Xe	0.870	0.022	^{129}Ba	0.860	0.022
^{124}Xe	0.900	0.014	^{130}Ba	0.890	0.014
^{125}Xe	0.930	0.014	^{131}Ba	0.880	0.022
^{126}Xe	0.930	0.014	^{132}Ba	0.920	0.014
^{127}Xe	0.950	0.014	^{133}Ba	0.920	0.014
^{128}Xe	0.960	0.014	^{134}Ba	0.930	0.028

TABLE VI: Recoil velocities of fission fragments (in cm/ns) measured in the frame of the fissioning system for the reaction ^{238}U(1A GeV)+d, with their total error.

nucleus	v_{fiss} (cm/ns)	ε_{tot} (cm/ns)	nucleus	v_{fiss} (cm/ns)	ε_{tot} (cm/ns)
^{135}Ba	0.910	0.020	^{142}Ce	0.870	0.014
^{136}Ba	0.900	0.014	^{143}Ce	0.880	0.014
^{137}Ba	0.920	0.014	^{144}Ce	0.860	0.014
^{138}Ba	0.910	0.014	^{145}Ce	0.860	0.022
^{139}Ba	0.910	0.014	^{146}Ce	0.860	0.022
^{140}Ba	0.920	0.014	^{147}Ce	0.860	0.014
^{141}Ba	0.910	0.014	^{148}Ce	0.860	0.014
^{142}Ba	0.920	0.014	^{149}Ce	0.870	0.014
^{143}Ba	0.910	0.014	^{150}Ce	0.870	0.014
^{144}Ba	0.910	0.014	^{151}Ce	0.850	0.022
^{145}Ba	0.890	0.014	^{152}Ce	0.850	0.050
^{146}Ba	0.890	0.014	^{128}Pr	0.450	0.130
^{147}Ba	0.890	0.022	^{129}Pr	0.550	0.100
^{148}Ba	0.890	0.022	^{130}Pr	0.590	0.080
^{124}La	0.440	0.200	^{131}Pr	0.660	0.032
^{125}La	0.610	0.090	^{132}Pr	0.690	0.014
^{126}La	0.680	0.051	^{133}Pr	0.720	0.014
^{127}La	0.700	0.041	^{134}Pr	0.740	0.014
^{128}La	0.720	0.014	^{135}Pr	0.750	0.022
^{129}La	0.750	0.014	^{136}Pr	0.750	0.014
^{130}La	0.790	0.041	^{137}Pr	0.780	0.014
^{131}La	0.810	0.014	^{138}Pr	0.770	0.022
^{132}La	0.840	0.014	^{139}Pr	0.790	0.014
^{133}La	0.850	0.014	^{140}Pr	0.810	0.014
^{134}La	0.860	0.014	^{141}Pr	0.820	0.014
^{135}La	0.860	0.014	^{142}Pr	0.820	0.022
^{136}La	0.870	0.014	^{143}Pr	0.840	0.014
^{137}La	0.860	0.014	^{144}Pr	0.850	0.014
^{138}La	0.860	0.014	^{145}Pr	0.860	0.014
^{139}La	0.860	0.014	^{146}Pr	0.860	0.014
^{140}La	0.870	0.014	^{147}Pr	0.850	0.014
^{141}La	0.860	0.032	^{148}Pr	0.860	0.014
^{142}La	0.870	0.014	^{149}Pr	0.840	0.022
^{143}La	0.870	0.014	^{150}Pr	0.850	0.014
^{144}La	0.860	0.032	^{151}Pr	0.840	0.014
^{145}La	0.880	0.014	^{152}Pr	0.850	0.010
^{146}La	0.870	0.014	^{153}Pr	0.840	0.014
^{147}La	0.870	0.014	^{154}Pr	0.850	0.050
^{148}La	0.860	0.014	^{131}Nd	0.430	0.150
^{149}La	0.880	0.014	^{132}Nd	0.560	0.120
^{150}La	0.880	0.061	^{133}Nd	0.630	0.071
^{126}Ce	0.360	0.230	^{134}Nd	0.670	0.022
^{127}Ce	0.540	0.100	^{135}Nd	0.700	0.014
^{128}Ce	0.660	0.030	^{136}Nd	0.720	0.036
^{129}Ce	0.710	0.014	^{137}Nd	0.730	0.041
^{130}Ce	0.750	0.022	^{138}Nd	0.740	0.022
^{131}Ce	0.780	0.022	^{139}Nd	0.740	0.014
^{132}Ce	0.810	0.032	^{140}Nd	0.740	0.014
^{133}Ce	0.810	0.022	^{141}Nd	0.750	0.014
^{134}Ce	0.830	0.014	^{142}Nd	0.780	0.014
^{135}Ce	0.840	0.014	^{142}Nd	0.780	0.014
^{136}Ce	0.840	0.014	^{143}Nd	0.760	0.014
^{137}Ce	0.860	0.014	^{144}Nd	0.790	0.014
^{138}Ce	0.860	0.014	^{145}Nd	0.800	0.010
^{139}Ce	0.850	0.014	^{146}Nd	0.800	0.022
^{140}Ce	0.860	0.014	^{147}Nd	0.810	0.014
^{141}Ce	0.860	0.014	^{148}Nd	0.820	0.014

TABLE VII: Recoil velocities of fission fragments (in cm/ns) measured in the frame of the fissioning system for the reaction ^{238}U(1A GeV)+d, with their total error.

nucleus	v_{fiss} (cm/ns)	ε_{tot} (cm/ns)	nucleus	v_{fiss} (cm/ns)	ε_{tot} (cm/ns)
^{149}Nd	0.820	0.014	^{148}Eu	0.690	0.041
^{150}Nd	0.830	0.022	^{149}Eu	0.700	0.040
^{151}Nd	0.830	0.022	^{150}Eu	0.710	0.014
^{152}Nd	0.830	0.051	^{151}Eu	0.720	0.010
^{153}Nd	0.810	0.041	^{152}Eu	0.710	0.014
^{154}Nd	0.800	0.051	^{153}Eu	0.720	0.014
^{155}Nd	0.810	0.022	^{154}Eu	0.750	0.040
^{156}Nd	0.820	0.014	^{155}Eu	0.750	0.022
^{133}Pm	0.460	0.150	^{156}Eu	0.750	0.010
^{134}Pm	0.520	0.120	^{157}Eu	0.750	0.041
^{135}Pm	0.590	0.080	^{149}Gd	0.640	0.051
^{136}Pm	0.650	0.030	^{150}Gd	0.640	0.041
^{137}Pm	0.670	0.032	^{151}Gd	0.670	0.041
^{138}Pm	0.700	0.028	^{152}Gd	0.690	0.010
^{139}Pm	0.690	0.030	^{153}Gd	0.670	0.022
^{140}Pm	0.740	0.014	^{154}Gd	0.700	0.041
^{141}Pm	0.760	0.014	^{155}Gd	0.700	0.014
^{142}Pm	0.780	0.014	^{156}Gd	0.710	0.014
^{143}Pm	0.760	0.022	^{157}Gd	0.720	0.014
^{144}Pm	0.800	0.022	^{158}Gd	0.710	0.032
^{145}Pm	0.770	0.022	^{159}Gd	0.710	0.022
^{146}Pm	0.790	0.014	^{154}Tb	0.680	0.032
^{147}Pm	0.810	0.014	^{155}Tb	0.690	0.030
^{148}Pm	0.820	0.014	^{156}Tb	0.700	0.010
^{149}Pm	0.830	0.014	^{157}Tb	0.700	0.010
^{150}Pm	0.810	0.014	^{158}Tb	0.690	0.050
^{151}Pm	0.820	0.014	^{159}Tb	0.700	0.022
^{152}Pm	0.810	0.014	^{160}Tb	0.700	0.020
^{153}Pm	0.800	0.022	^{156}Dy	0.660	0.061
^{154}Pm	0.810	0.032	^{157}Dy	0.660	0.051
^{155}Pm	0.800	0.064	^{158}Dy	0.650	0.032
^{156}Pm	0.810	0.022	^{159}Dy	0.670	0.010
^{157}Pm	0.810	0.014	^{160}Dy	0.660	0.051
^{158}Pm	0.800	0.022	^{161}Dy	0.670	0.010
^{139}Sm	0.600	0.050	^{162}Dy	0.670	0.060
^{140}Sm	0.630	0.060			
^{141}Sm	0.650	0.032			
^{142}Sm	0.690	0.022			
^{143}Sm	0.710	0.022			
^{144}Sm	0.730	0.014			
^{145}Sm	0.730	0.014			
^{146}Sm	0.740	0.014			
^{147}Sm	0.740	0.022			
^{148}Sm	0.760	0.014			
^{149}Sm	0.760	0.014			
^{150}Sm	0.760	0.014			
^{151}Sm	0.760	0.014			
^{152}Sm	0.760	0.014			
^{153}Sm	0.770	0.010			
^{154}Sm	0.780	0.014			
^{155}Sm	0.780	0.014			
^{156}Sm	0.770	0.022			
^{157}Sm	0.770	0.032			
^{158}Sm	0.760	0.061			
^{159}Sm	0.770	0.022			
^{160}Sm	0.770	0.032			
^{147}Eu	0.660	0.051			

TABLE VIII: Recoil velocities of fission fragments (in cm/ns) measured in the frame of the fissioning system for the reaction ^{238}U(1A GeV)+d, with their total error.

nucleus	σ (mb)	ε_{STAT} (mb)	ε_{SYST} (mb)	nucleus	σ (mb)	ε_{STAT} (mb)	ε_{SYST} (mb)
^{49}V	0.159	0.003	0.021	^{65}Ni	3.886	0.096	0.774
^{50}V	0.770	0.013	0.099	^{66}Ni	2.549	0.094	0.508
^{51}V	1.771	0.040	0.226	^{67}Ni	1.745	0.087	0.348
^{52}V	1.618	0.059	0.091	^{68}Ni	0.770	0.054	0.073
^{53}V	1.470	0.074	0.083	^{69}Ni	0.437	0.032	0.090
^{54}V	0.973	0.078	0.123	^{70}Ni	0.129	0.012	0.015
^{55}V	0.411	0.053	0.054	^{59}Cu	0.005	0.001	0.002
^{56}V	0.219	0.037	0.032	^{60}Cu	0.051	0.002	0.018
^{57}V	0.019	0.003	0.002	^{61}Cu	0.505	0.007	0.125
^{51}Cr	0.375	0.005	0.059	^{62}Cu	1.714	0.015	0.379
^{52}Cr	1.333	0.017	0.202	^{63}Cu	3.304	0.028	0.696
^{53}Cr	2.373	0.042	0.361	^{64}Cu	4.286	0.044	0.895
^{54}Cr	2.485	0.061	0.377	^{65}Cu	5.252	0.067	1.099
^{55}Cr	2.044	0.082	0.310	^{66}Cu	5.299	0.085	1.107
^{56}Cr	1.331	0.074	0.202	^{67}Cu	4.369	0.089	0.932
^{57}Cr	0.551	0.053	0.037	^{68}Cu	3.783	0.106	0.815
^{58}Cr	0.281	0.037	0.020	^{69}Cu	2.698	0.101	0.563
^{59}Cr	0.068	0.010	0.007	^{70}Cu	1.376	0.072	0.290
^{53}Mn	0.536	0.007	0.094	^{71}Cu	1.094	0.062	0.104
^{54}Mn	1.731	0.019	0.292	^{72}Cu	0.437	0.027	0.092
^{55}Mn	2.683	0.037	0.452	^{73}Cu	0.208	0.014	0.024
^{56}Mn	2.725	0.056	0.463	^{74}Cu	0.082	0.006	0.010
^{57}Mn	2.833	0.082	0.478	^{62}Zn	0.020	0.001	0.004
^{58}Mn	1.808	0.073	0.304	^{63}Zn	0.308	0.004	0.069
^{59}Mn	1.263	0.074	0.213	^{64}Zn	1.356	0.012	0.293
^{60}Mn	0.516	0.050	0.086	^{65}Zn	3.039	0.024	0.659
^{61}Mn	0.283	0.029	0.048	^{66}Zn	4.647	0.043	1.006
^{62}Mn	0.076	0.010	0.008	^{67}Zn	6.196	0.070	1.339
^{55}Fe	0.435	0.005	0.081	^{68}Zn	6.349	0.088	1.373
^{56}Fe	2.011	0.019	0.363	^{69}Zn	5.969	0.102	1.291
^{57}Fe	2.755	0.033	0.496	^{70}Zn	5.093	0.111	1.145
^{58}Fe	3.539	0.056	0.639	^{71}Zn	4.100	0.117	0.887
^{59}Fe	2.779	0.064	0.530	^{72}Zn	2.448	0.095	0.532
^{60}Fe	2.529	0.079	0.457	^{73}Zn	1.227	0.063	0.120
^{61}Fe	1.864	0.084	0.336	^{74}Zn	0.851	0.040	0.082
^{62}Fe	0.875	0.059	0.158	^{75}Zn	0.421	0.022	0.092
^{63}Fe	0.364	0.037	0.068	^{76}Zn	0.119	0.006	0.027
^{64}Fe	0.124	0.013	0.014	^{77}Zn	0.051	0.003	0.012
^{65}Fe	0.012	0.001	0.008	^{78}Zn	0.018	0.001	0.005
^{57}Co	0.112	0.001	0.023	^{65}Ga	0.084	0.001	0.020
^{58}Co	1.427	0.013	0.271	^{66}Ga	0.723	0.007	0.177
^{59}Co	3.057	0.030	0.588	^{67}Ga	2.460	0.020	0.537
^{60}Co	3.476	0.047	0.670	^{68}Ga	4.325	0.039	0.923
^{61}Co	3.503	0.062	0.696	^{69}Ga	6.319	0.066	1.349
^{62}Co	3.279	0.081	0.623	^{70}Ga	7.708	0.094	1.654
^{63}Co	2.533	0.083	0.500	^{71}Ga	8.182	0.115	1.749
^{64}Co	1.800	0.087	0.342	^{72}Ga	6.917	0.121	1.501
^{65}Co	0.846	0.062	0.163	^{73}Ga	5.710	0.132	1.218
^{66}Co	0.386	0.030	0.073	^{74}Ga	3.891	0.120	0.831
^{67}Co	0.266	0.023	0.052	^{75}Ga	1.962	0.084	0.448
^{68}Co	0.095	0.010	0.011	^{76}Ga	1.663	0.065	0.159
^{69}Co	0.042	0.005	0.006	^{77}Ga	0.879	0.031	0.197
^{60}Ni	0.567	0.005	0.114	^{78}Ga	0.422	0.020	0.056
^{61}Ni	2.768	0.025	0.559	^{79}Ga	0.291	0.011	0.037
^{62}Ni	3.370	0.037	0.673	^{80}Ga	0.119	0.005	0.014
^{63}Ni	4.156	0.063	0.830	^{67}Ge	0.073	0.001	0.018
^{64}Ni	3.916	0.075	0.816	^{68}Ge	0.465	0.005	0.122

TABLE IX: Isotopic cross-sections of spallation-evaporation fragments of ^{238}U(1A GeV)+d, with their statistical and systematic uncertainties.

nucleus	σ (mb)	ε_{STAT} (mb)	ε_{SYST} (mb)	nucleus	σ (mb)	ε_{STAT} (mb)	ε_{SYST} (mb)
^{69}Ge	2.159	0.018	0.515	^{78}Br	7.264	0.069	1.694
^{70}Ge	3.997	0.033	0.903	^{79}Br	10.398	0.100	2.416
^{71}Ge	6.243	0.061	1.379	^{80}Br	12.284	0.124	2.852
^{72}Ge	8.447	0.090	1.868	^{81}Br	14.471	0.162	3.359
^{73}Ge	9.475	0.118	2.091	^{82}Br	12.041	0.163	2.797
^{74}Ge	8.801	0.128	1.969	^{83}Br	10.773	0.174	2.484
^{75}Ge	7.405	0.142	1.637	^{84}Br	8.430	0.166	1.943
^{76}Ge	5.796	0.134	1.305	^{85}Br	5.936	0.153	0.705
^{77}Ge	4.048	0.121	0.922	^{86}Br	5.630	0.103	0.591
^{78}Ge	2.438	0.088	0.254	^{87}Br	5.336	0.078	0.548
^{79}Ge	1.470	0.045	0.158	^{88}Br	3.583	0.054	0.826
^{80}Ge	1.255	0.034	0.277	^{89}Br	2.128	0.032	0.492
^{81}Ge	0.712	0.020	0.158	^{90}Br	0.791	0.014	0.181
^{82}Ge	0.450	0.012	0.100	^{91}Br	0.317	0.006	0.040
^{83}Ge	0.151	0.004	0.020	^{92}Br	0.070	0.003	0.011
^{69}As	0.053	0.001	0.013	^{76}Kr	0.081	0.001	0.021
^{70}As	0.481	0.006	0.109	^{77}Kr	0.790	0.009	0.196
^{71}As	1.600	0.014	0.359	^{78}Kr	2.056	0.018	0.482
^{72}As	3.586	0.030	0.801	^{79}Kr	3.965	0.035	0.904
^{73}As	6.194	0.056	1.381	^{80}Kr	6.672	0.059	1.532
^{74}As	7.688	0.079	1.715	^{81}Kr	10.931	0.099	2.492
^{75}As	10.819	0.119	2.438	^{82}Kr	13.344	0.120	3.090
^{76}As	10.065	0.131	2.246	^{83}Kr	16.319	0.166	3.724
^{77}As	10.433	0.157	2.328	^{84}Kr	15.467	0.183	3.549
^{78}As	7.783	0.151	1.738	^{85}Kr	13.574	0.186	3.095
^{79}As	5.915	0.138	1.374	^{86}Kr	10.429	0.172	2.420
^{80}As	4.191	0.138	0.430	^{87}Kr	8.922	0.172	2.033
^{81}As	2.890	0.073	0.292	^{88}Kr	8.752	0.173	0.917
^{82}As	2.235	0.050	0.222	^{89}Kr	6.873	0.093	0.705
^{83}As	1.688	0.038	0.377	^{90}Kr	5.934	0.069	1.356
^{84}As	0.434	0.010	0.097	^{91}Kr	3.999	0.055	0.912
^{85}As	0.262	0.006	0.059	^{92}Kr	1.925	0.025	0.440
^{86}As	0.131	0.004	0.017	^{93}Kr	0.709	0.011	0.161
^{71}Se	0.031	0.001	0.009	^{94}Kr	0.225	0.005	0.029
^{72}Se	0.329	0.004	0.085	^{95}Kr	0.055	0.002	0.008
^{73}Se	1.369	0.012	0.315	^{78}Rb	0.037	0.001	0.009
^{74}Se	3.053	0.025	0.703	^{79}Rb	0.458	0.006	0.114
^{75}Se	5.501	0.047	1.269	^{80}Rb	1.572	0.015	0.376
^{76}Se	7.932	0.075	1.828	^{81}Rb	3.455	0.029	0.810
^{77}Se	10.228	0.108	2.358	^{82}Rb	6.654	0.058	1.521
^{78}Se	12.497	0.136	2.879	^{83}Rb	10.221	0.087	2.359
^{79}Se	12.054	0.160	2.780	^{84}Rb	14.326	0.123	3.316
^{80}Se	10.764	0.167	2.481	^{85}Rb	17.249	0.157	4.034
^{81}Se	8.513	0.162	1.963	^{86}Rb	17.218	0.184	3.963
^{82}Se	6.492	0.149	1.498	^{87}Rb	15.941	0.191	3.634
^{83}Se	4.949	0.124	0.520	^{88}Rb	12.739	0.185	2.926
^{84}Se	4.022	0.073	0.429	^{89}Rb	11.586	0.191	2.664
^{85}Se	3.034	0.050	0.698	^{90}Rb	9.864	0.211	1.040
^{86}Se	2.200	0.040	0.509	^{91}Rb	8.898	0.129	0.944
^{87}Se	1.016	0.018	0.234	^{92}Rb	7.201	0.088	0.753
^{88}Se	0.463	0.009	0.060	^{93}Rb	5.593	0.065	1.276
^{89}Se	0.130	0.004	0.017	^{94}Rb	3.166	0.044	0.722
^{73}Br	0.012	0.000	0.003	^{95}Rb	1.536	0.021	0.351
^{74}Br	0.164	0.003	0.044	^{96}Rb	0.510	0.009	0.116
^{75}Br	0.962	0.010	0.236	^{97}Rb	0.217	0.005	0.028
^{76}Br	2.496	0.021	0.581	^{80}Sr	0.030	0.001	0.008
^{77}Br	4.120	0.035	0.949	^{81}Sr	0.324	0.005	0.106

TABLE X: Isotopic cross-sections of spallation-evaporation fragments of ^{238}U(1A GeV)+d, with their statistical and systematic uncertainties.

nucleus	σ (mb)	ε_{STAT} (mb)	ε_{SYST} (mb)	nucleus	σ (mb)	ε_{STAT} (mb)	ε_{SYST} (mb)
^{82}Sr	0.864	0.009	0.225	^{101}Zr	5.516	0.061	0.579
^{83}Sr	2.878	0.026	0.673	^{102}Zr	3.289	0.040	0.757
^{84}Sr	5.304	0.045	1.258	^{103}Zr	1.150	0.017	0.266
^{85}Sr	9.982	0.085	2.306	^{104}Zr	0.414	0.008	0.095
^{86}Sr	13.913	0.114	3.182	^{105}Zr	0.093	0.003	0.013
^{87}Sr	17.897	0.149	4.076	^{87}Nb	0.106	0.002	0.033
^{88}Sr	18.938	0.188	4.369	^{88}Nb	0.445	0.006	0.125
^{89}Sr	18.306	0.200	4.197	^{89}Nb	1.422	0.015	0.332
^{90}Sr	15.109	0.195	3.445	^{90}Nb	3.462	0.031	0.811
^{91}Sr	13.863	0.203	3.162	^{91}Nb	7.335	0.060	1.688
^{92}Sr	12.004	0.200	2.739	^{92}Nb	10.170	0.084	2.395
^{93}Sr	10.979	0.202	1.175	^{93}Nb	13.121	0.109	3.029
^{94}Sr	10.720	0.125	1.122	^{94}Nb	15.875	0.137	3.678
^{95}Sr	7.233	0.076	1.658	^{95}Nb	19.255	0.182	4.458
^{96}Sr	5.207	0.060	1.187	^{96}Nb	18.550	0.188	4.284
^{97}Sr	2.715	0.033	0.619	^{97}Nb	17.958	0.199	4.131
^{98}Sr	1.344	0.018	0.306	^{98}Nb	16.911	0.211	3.923
^{99}Sr	0.343	0.007	0.044	^{99}Nb	16.133	0.217	3.718
^{100}Sr	0.116	0.003	0.015	^{100}Nb	14.169	0.236	1.502
^{82}Y	0.037	0.001	0.016	^{101}Nb	13.049	0.170	1.411
^{83}Y	0.200	0.003	0.072	^{102}Nb	8.380	0.092	0.973
^{84}Y	0.825	0.010	0.200	^{103}Nb	7.247	0.072	0.762
^{85}Y	2.260	0.021	0.585	^{104}Nb	3.629	0.046	0.382
^{86}Y	5.244	0.045	1.221	^{105}Nb	1.913	0.027	0.240
^{87}Y	8.730	0.073	2.020	^{106}Nb	0.634	0.012	0.079
^{88}Y	14.169	0.116	3.286	^{107}Nb	0.223	0.005	0.029
^{89}Y	17.153	0.138	4.025	^{89}Mo	0.065	0.002	0.018
^{90}Y	18.829	0.174	4.335	^{90}Mo	0.188	0.003	0.043
^{91}Y	19.189	0.199	4.433	^{91}Mo	1.132	0.012	0.314
^{92}Y	17.069	0.200	3.926	^{92}Mo	2.744	0.025	0.623
^{93}Y	15.452	0.204	3.576	^{93}Mo	5.860	0.052	1.351
^{94}Y	14.498	0.214	3.343	^{94}Mo	8.661	0.075	1.979
^{95}Y	11.265	0.211	1.178	^{95}Mo	12.761	0.106	2.951
^{96}Y	10.508	0.141	1.308	^{96}Mo	15.633	0.132	3.630
^{97}Y	9.141	0.101	1.016	^{97}Mo	18.477	0.169	4.249
^{98}Y	6.172	0.067	1.421	^{98}Mo	20.955	0.200	4.798
^{99}Y	4.739	0.056	1.090	^{99}Mo	21.074	0.213	4.799
^{100}Y	1.918	0.025	0.441	^{100}Mo	20.067	0.226	4.564
^{101}Y	0.763	0.011	0.176	^{101}Mo	18.476	0.225	4.224
^{102}Y	0.216	0.005	0.028	^{102}Mo	17.654	0.233	4.035
^{84}Zr	0.005	0.000	0.001	^{103}Mo	14.549	0.240	1.532
^{85}Zr	0.141	0.003	0.034	^{104}Mo	11.788	0.127	1.323
^{86}Zr	0.394	0.005	0.094	^{105}Mo	7.935	0.088	0.833
^{87}Zr	1.842	0.018	0.433	^{106}Mo	5.116	0.057	0.534
^{88}Zr	3.849	0.033	0.926	^{107}Mo	2.385	0.037	0.543
^{89}Zr	8.169	0.066	1.905	^{108}Mo	1.131	0.019	0.257
^{90}Zr	12.143	0.097	2.831	^{109}Mo	0.344	0.009	0.043
^{91}Zr	16.194	0.132	3.759	^{110}Mo	0.119	0.004	0.015
^{92}Zr	17.942	0.157	4.158	^{91}Tc	0.045	0.001	0.010
^{93}Zr	18.508	0.185	4.290	^{92}Tc	0.246	0.004	0.069
^{94}Zr	18.217	0.195	4.190	^{93}Tc	0.855	0.010	0.217
^{95}Zr	17.963	0.215	4.137	^{94}Tc	2.397	0.024	0.550
^{96}Zr	15.344	0.208	3.533	^{95}Tc	4.171	0.039	0.969
^{97}Zr	14.472	0.216	3.333	^{96}Tc	6.673	0.062	1.555
^{98}Zr	13.364	0.229	1.443	^{97}Tc	9.851	0.085	2.316
^{99}Zr	11.323	0.125	1.275	^{98}Tc	14.187	0.120	3.322
^{100}Zr	9.751	0.093	1.061	^{99}Tc	16.592	0.147	3.869

TABLE XI: Isotopic cross-sections of spallation-evaporation fragments of ^{238}U(1A GeV)+d, with their statistical and systematic uncertainties.

nucleus	σ (mb)	ε_{STAT} (mb)	ε_{SYST} (mb)	nucleus	σ (mb)	ε_{STAT} (mb)	ε_{SYST} (mb)
^{100}Tc	19.663	0.185	4.508	^{118}Rh	0.070	0.003	0.010
^{101}Tc	20.179	0.197	4.609	^{98}Pd	0.002	0.000	0.000
^{102}Tc	18.649	0.200	4.313	^{99}Pd	0.191	0.004	0.054
^{103}Tc	21.048	0.231	4.807	^{100}Pd	0.727	0.010	0.175
^{104}Tc	17.382	0.224	3.960	^{101}Pd	1.862	0.022	0.485
^{105}Tc	16.068	0.224	3.658	^{102}Pd	3.455	0.037	0.854
^{106}Tc	11.778	0.170	1.345	^{103}Pd	5.816	0.057	1.394
^{107}Tc	10.211	0.111	1.119	^{104}Pd	8.667	0.080	2.125
^{108}Tc	5.921	0.067	0.618	^{105}Pd	11.983	0.108	2.835
^{109}Tc	3.708	0.045	0.387	^{106}Pd	14.443	0.134	3.394
^{110}Tc	1.718	0.029	0.211	^{107}Pd	17.980	0.167	4.203
^{111}Tc	0.751	0.014	0.093	^{108}Pd	19.669	0.194	4.581
^{93}Ru	0.020	0.001	0.005	^{109}Pd	19.397	0.198	4.516
^{94}Ru	0.026	0.001	0.008	^{110}Pd	18.034	0.198	4.195
^{95}Ru	0.583	0.008	0.136	^{111}Pd	17.787	0.212	4.109
^{96}Ru	1.588	0.018	0.394	^{112}Pd	17.657	0.215	4.071
^{97}Ru	3.631	0.037	0.872	^{113}Pd	14.161	0.202	2.715
^{98}Ru	5.619	0.053	1.327	^{114}Pd	10.619	0.139	1.200
^{99}Ru	8.850	0.080	2.063	^{115}Pd	7.617	0.092	0.918
^{100}Ru	12.199	0.104	2.846	^{116}Pd	4.432	0.053	0.509
^{101}Ru	16.912	0.148	3.880	^{117}Pd	2.208	0.032	0.233
^{102}Ru	18.222	0.165	4.239	^{118}Pd	1.174	0.024	0.124
^{103}Ru	19.590	0.189	4.497	^{119}Pd	0.460	0.011	0.057
^{104}Ru	19.782	0.198	4.625	^{120}Pd	0.136	0.005	0.019
^{105}Ru	19.489	0.211	4.523	^{100}Ag	0.012	0.000	0.002
^{106}Ru	19.459	0.229	4.438	^{101}Ag	0.076	0.002	0.019
^{107}Ru	17.368	0.224	3.954	^{102}Ag	0.471	0.007	0.113
^{108}Ru	15.723	0.232	1.703	^{103}Ag	1.229	0.016	0.282
^{109}Ru	10.755	0.134	1.212	^{104}Ag	2.326	0.026	0.574
^{110}Ru	8.438	0.096	0.963	^{105}Ag	3.769	0.040	0.969
^{111}Ru	4.769	0.057	0.497	^{106}Ag	6.369	0.062	1.491
^{112}Ru	2.682	0.039	0.334	^{107}Ag	9.757	0.092	2.382
^{113}Ru	1.017	0.021	0.125	^{108}Ag	12.643	0.120	2.950
^{114}Ru	0.437	0.011	0.053	^{109}Ag	15.100	0.143	3.501
^{115}Ru	0.122	0.004	0.015	^{110}Ag	16.290	0.165	3.756
^{96}Rh	0.030	0.001	0.013	^{111}Ag	18.021	0.183	4.161
^{97}Rh	0.268	0.004	0.101	^{112}Ag	17.368	0.192	3.998
^{98}Rh	1.005	0.012	0.240	^{113}Ag	17.722	0.203	4.065
^{99}Rh	2.145	0.023	0.540	^{114}Ag	16.645	0.205	3.794
^{100}Rh	4.265	0.043	0.981	^{115}Ag	15.805	0.194	3.593
^{101}Rh	6.882	0.064	1.586	^{116}Ag	12.694	0.194	1.481
^{102}Rh	10.234	0.092	2.376	^{117}Ag	9.756	0.115	1.180
^{103}Rh	14.602	0.126	3.401	^{118}Ag	6.062	0.074	0.685
^{104}Rh	17.064	0.157	3.942	^{119}Ag	3.861	0.048	0.410
^{105}Rh	20.457	0.189	4.716	^{120}Ag	1.616	0.026	0.174
^{106}Rh	19.515	0.196	4.499	^{121}Ag	0.809	0.017	0.098
^{107}Rh	20.153	0.206	4.611	^{122}Ag	0.264	0.008	0.034
^{108}Rh	18.780	0.215	4.298	^{103}Cd	0.019	0.001	0.005
^{109}Rh	16.913	0.202	4.612	^{104}Cd	0.254	0.005	0.061
^{110}Rh	15.025	0.200	1.576	^{105}Cd	0.843	0.012	0.280
^{111}Rh	13.508	0.197	1.593	^{106}Cd	1.709	0.021	0.462
^{112}Rh	10.379	0.120	1.238	^{107}Cd	3.123	0.034	0.781
^{113}Rh	6.707	0.076	0.795	^{108}Cd	4.959	0.052	1.283
^{114}Rh	3.412	0.044	0.359	^{109}Cd	7.643	0.076	1.795
^{115}Rh	1.745	0.030	0.215	^{110}Cd	9.638	0.095	2.276
^{116}Rh	0.685	0.015	0.083	^{111}Cd	12.226	0.120	2.817
^{117}Rh	0.251	0.007	0.032	^{112}Cd	14.366	0.145	3.283

TABLE XII: Isotopic cross-sections of spallation-evaporation fragments of ^{238}U(1A GeV)+d, with their statistical and systematic uncertainties.

nucleus	σ (mb)	ε_{STAT} (mb)	ε_{SYST} (mb)	nucleus	σ (mb)	ε_{STAT} (mb)	ε_{SYST} (mb)
^{113}Cd	15.128	0.160	3.435	^{126}Sn	3.669	0.049	0.413
^{114}Cd	15.777	0.171	3.600	^{127}Sn	2.771	0.036	0.297
^{115}Cd	16.475	0.190	3.731	^{128}Sn	1.820	0.026	0.196
^{116}Cd	16.740	0.203	3.761	^{129}Sn	1.343	0.019	0.166
^{117}Cd	15.113	0.190	3.410	^{130}Sn	1.169	0.014	0.144
^{118}Cd	10.934	0.156	2.513	^{131}Sn	0.733	0.008	0.091
^{119}Cd	10.290	0.153	1.115	^{132}Sn	0.442	0.006	0.055
^{120}Cd	7.704	0.096	0.801	^{133}Sn	0.012	0.000	0.004
^{121}Cd	4.621	0.059	0.562	^{109}Sb	0.009	0.001	0.002
^{122}Cd	2.467	0.035	0.257	^{110}Sb	0.057	0.002	0.014
^{123}Cd	1.327	0.026	0.140	^{111}Sb	0.168	0.005	0.042
^{124}Cd	0.510	0.012	0.062	^{112}Sb	0.570	0.010	0.139
^{125}Cd	0.203	0.006	0.025	^{113}Sb	1.178	0.017	0.295
^{126}Cd	0.077	0.003	0.010	^{114}Sb	2.131	0.029	0.513
^{105}In	0.013	0.000	0.003	^{115}Sb	3.333	0.040	0.842
^{106}In	0.114	0.003	0.029	^{116}Sb	5.252	0.062	1.347
^{107}In	0.452	0.008	0.118	^{117}Sb	6.393	0.077	1.650
^{108}In	1.084	0.015	0.265	^{118}Sb	8.164	0.094	2.079
^{109}In	2.088	0.025	0.503	^{119}Sb	9.653	0.114	2.350
^{110}In	3.877	0.042	0.975	^{120}Sb	10.961	0.132	2.603
^{111}In	5.395	0.055	1.385	^{121}Sb	11.627	0.143	2.747
^{112}In	7.881	0.082	2.007	^{122}Sb	11.060	0.144	2.570
^{113}In	10.381	0.105	2.550	^{123}Sb	11.611	0.156	2.688
^{114}In	12.574	0.130	2.968	^{124}Sb	10.784	0.147	2.481
^{115}In	13.844	0.151	3.296	^{125}Sb	9.661	0.134	2.221
^{116}In	15.444	0.171	3.592	^{126}Sb	7.116	0.119	1.633
^{117}In	15.690	0.178	3.638	^{127}Sb	6.640	0.104	0.716
^{118}In	14.787	0.183	3.407	^{128}Sb	5.094	0.068	0.579
^{119}In	13.862	0.176	3.192	^{129}Sb	3.929	0.047	0.423
^{120}In	12.203	0.159	2.811	^{130}Sb	3.203	0.037	0.344
^{121}In	10.288	0.166	1.109	^{131}Sb	3.059	0.034	0.703
^{122}In	8.373	0.117	0.947	^{132}Sb	2.227	0.023	0.274
^{123}In	6.136	0.080	0.694	^{133}Sb	1.720	0.017	0.212
^{124}In	3.472	0.047	0.378	^{134}Sb	0.096	0.001	0.026
^{125}In	1.783	0.027	0.191	^{135}Sb	0.029	0.001	0.009
^{126}In	0.968	0.020	0.103	^{112}Te	0.024	0.001	0.007
^{127}In	0.548	0.012	0.068	^{113}Te	0.115	0.003	0.027
^{128}In	0.038	0.001	0.009	^{114}Te	0.329	0.007	0.079
^{107}Sn	0.008	0.001	0.002	^{115}Te	0.841	0.014	0.205
^{108}Sn	0.034	0.001	0.009	^{116}Te	1.537	0.021	0.387
^{109}Sn	0.281	0.006	0.064	^{117}Te	2.559	0.034	0.620
^{110}Sn	0.727	0.011	0.177	^{118}Te	3.488	0.046	0.910
^{111}Sn	1.822	0.023	0.440	^{119}Te	4.839	0.063	1.246
^{112}Sn	2.825	0.033	0.735	^{120}Te	6.182	0.077	1.655
^{113}Sn	4.408	0.051	1.103	^{121}Te	6.582	0.086	1.664
^{114}Sn	6.598	0.073	1.689	^{122}Te	8.342	0.110	2.066
^{115}Sn	8.391	0.091	2.113	^{123}Te	9.281	0.127	2.194
^{116}Sn	9.622	0.105	2.406	^{124}Te	8.650	0.124	2.087
^{117}Sn	11.996	0.134	2.826	^{125}Te	9.477	0.139	2.215
^{118}Sn	11.668	0.134	2.781	^{126}Te	9.294	0.137	2.143
^{119}Sn	12.795	0.150	3.035	^{127}Te	8.778	0.128	2.022
^{120}Sn	12.038	0.156	2.769	^{128}Te	6.930	0.106	0.761
^{121}Sn	12.193	0.159	2.814	^{129}Te	6.561	0.122	0.717
^{122}Sn	11.054	0.146	2.555	^{130}Te	5.171	0.071	0.557
^{123}Sn	9.376	0.136	1.003	^{131}Te	4.740	0.057	0.549
^{124}Sn	7.555	0.127	0.867	^{132}Te	4.721	0.047	0.531
^{125}Sn	5.881	0.078	0.682	^{133}Te	4.802	0.041	0.518

TABLE XIII: Isotopic cross-sections of spallation-evaporation fragments of ^{238}U(1A GeV)+d, with their statistical and systematic uncertainties.

nucleus	σ (mb)	ε_{STAT} (mb)	ε_{SYST} (mb)	nucleus	σ (mb)	ε_{STAT} (mb)	ε_{SYST} (mb)
^{120}Sb	10.961	0.132	2.603	^{128}I	7.208	0.115	1.652
^{121}Sb	11.627	0.143	2.747	^{129}I	7.704	0.117	1.782
^{122}Sb	11.060	0.144	2.570	^{130}I	7.240	0.114	1.665
^{123}Sb	11.611	0.156	2.688	^{131}I	5.971	0.106	0.644
^{124}Sb	10.784	0.147	2.481	^{132}I	5.263	0.095	0.576
^{125}Sb	9.661	0.134	2.221	^{133}I	5.618	0.071	0.643
^{126}Sb	7.116	0.119	1.633	^{134}I	5.121	0.055	0.572
^{127}Sb	6.640	0.104	0.716	^{135}I	5.569	0.048	0.599
^{128}Sb	5.094	0.068	0.579	^{136}I	3.343	0.033	0.361
^{129}Sb	3.929	0.047	0.423	^{137}I	2.724	0.029	0.333
^{130}Sb	3.203	0.037	0.344	^{138}I	1.472	0.017	0.181
^{131}Sb	3.059	0.034	0.703	^{139}I	0.139	0.002	0.034
^{132}Sb	2.227	0.023	0.274	^{140}I	0.035	0.001	0.009
^{133}Sb	1.720	0.017	0.212	^{141}I	0.011	0.000	0.003
^{134}Sb	0.096	0.001	0.026	^{117}Xe	0.042	0.002	0.009
^{135}Sb	0.029	0.001	0.009	^{118}Xe	0.131	0.004	0.030
^{112}Te	0.024	0.001	0.007	^{119}Xe	0.403	0.009	0.101
^{113}Te	0.115	0.003	0.027	^{120}Xe	0.920	0.015	0.222
^{114}Te	0.329	0.007	0.079	^{121}Xe	1.578	0.024	0.455
^{115}Te	0.841	0.014	0.205	^{122}Xe	2.034	0.030	0.581
^{116}Te	1.537	0.021	0.387	^{123}Xe	2.824	0.043	0.797
^{117}Te	2.559	0.034	0.620	^{124}Xe	3.999	0.059	1.067
^{118}Te	3.488	0.046	0.910	^{125}Xe	5.219	0.076	1.345
^{119}Te	4.839	0.063	1.246	^{126}Xe	4.898	0.074	1.363
^{120}Te	6.182	0.077	1.655	^{127}Xe	6.186	0.096	1.540
^{121}Te	6.582	0.086	1.664	^{128}Xe	6.546	0.104	1.606
^{122}Te	8.342	0.110	2.066	^{129}Xe	6.572	0.108	1.576
^{123}Te	9.281	0.127	2.194	^{130}Xe	6.786	0.114	1.612
^{124}Te	8.650	0.124	2.087	^{131}Xe	6.535	0.109	1.541
^{125}Te	9.477	0.139	2.215	^{132}Xe	6.230	0.105	1.432
^{126}Te	9.294	0.137	2.143	^{133}Xe	5.988	0.100	0.647
^{127}Te	8.778	0.128	2.022	^{134}Xe	5.450	0.107	0.601
^{128}Te	6.930	0.106	0.761	^{135}Xe	6.154	0.088	0.668
^{129}Te	6.561	0.122	0.717	^{136}Xe	6.596	0.073	0.755
^{130}Te	5.171	0.071	0.557	^{137}Xe	5.196	0.052	0.562
^{131}Te	4.740	0.057	0.549	^{138}Xe	4.648	0.041	0.500
^{132}Te	4.721	0.047	0.531	^{139}Xe	2.848	0.027	0.309
^{133}Te	4.802	0.041	0.518	^{140}Xe	2.108	0.022	0.256
^{134}Te	4.534	0.040	0.557	^{141}Xe	1.030	0.013	0.128
^{135}Te	2.009	0.020	0.247	^{142}Xe	0.071	0.001	0.019
^{136}Te	0.202	0.002	0.051	^{143}Xe	0.015	0.000	0.005
^{137}Te	0.075	0.001	0.021	^{119}Cs	0.022	0.001	0.005
^{138}Te	0.023	0.001	0.006	^{120}Cs	0.088	0.003	0.021
^{139}Te	0.004	0.000	0.001	^{121}Cs	0.258	0.006	0.065
^{115}I	0.064	0.003	0.013	^{122}Cs	0.630	0.012	0.153
^{116}I	0.183	0.005	0.047	^{123}Cs	1.102	0.019	0.288
^{117}I	0.602	0.012	0.138	^{124}Cs	1.756	0.028	0.467
^{118}I	1.204	0.020	0.312	^{125}Cs	2.181	0.034	0.646
^{119}I	2.044	0.029	0.547	^{126}Cs	3.203	0.050	0.937
^{120}I	3.138	0.044	0.816	^{127}Cs	3.385	0.054	1.040
^{121}I	4.010	0.056	1.004	^{128}Cs	4.366	0.068	1.172
^{122}I	5.062	0.069	1.332	^{129}Cs	4.306	0.070	1.169
^{123}I	5.559	0.076	1.501	^{130}Cs	5.149	0.088	1.244
^{124}I	6.889	0.098	1.682	^{131}Cs	4.911	0.087	1.187
^{125}I	7.440	0.109	1.822	^{132}Cs	4.952	0.090	1.166
^{126}I	8.073	0.116	1.893	^{133}Cs	4.893	0.089	1.131
^{127}I	7.588	0.115	1.784	^{134}Cs	4.654	0.084	1.065

TABLE XIV: Isotopic cross-sections of spallation-evaporation fragments of ^{238}U(1A GeV)+d, with their statistical and systematic uncertainties.

nucleus	σ (mb)	ε_{STAT} (mb)	ε_{SYST} (mb)	nucleus	σ (mb)	ε_{STAT} (mb)	ε_{SYST} (mb)
^{135}Cs	4.548	0.082	1.046	^{141}La	1.842	0.046	0.199
^{136}Cs	4.116	0.077	0.455	^{142}La	2.120	0.058	0.232
^{137}Cs	4.331	0.084	0.510	^{143}La	2.106	0.042	0.230
^{138}Cs	3.844	0.056	0.423	^{144}La	1.937	0.034	0.217
^{139}Cs	3.495	0.042	0.407	^{145}La	2.074	0.028	0.248
^{140}Cs	3.494	0.036	0.379	^{146}La	1.200	0.017	0.144
^{141}Cs	3.116	0.029	0.338	^{147}La	1.175	0.017	0.142
^{142}Cs	1.978	0.022	0.215	^{148}La	0.458	0.010	0.056
^{143}Cs	0.648	0.008	0.150	^{149}La	0.059	0.002	0.014
^{144}Cs	0.122	0.002	0.031	^{150}La	0.013	0.001	0.004
^{145}Cs	0.035	0.001	0.009	^{126}Ce	0.023	0.001	0.006
^{146}Cs	0.008	0.000	0.002	^{127}Ce	0.086	0.003	0.020
^{121}Ba	0.016	0.001	0.004	^{128}Ce	0.233	0.006	0.067
^{122}Ba	0.064	0.002	0.014	^{129}Ce	0.602	0.013	0.153
^{123}Ba	0.199	0.005	0.049	^{130}Ce	0.794	0.016	0.307
^{124}Ba	0.397	0.009	0.127	^{131}Ce	1.213	0.023	0.435
^{125}Ba	0.822	0.016	0.225	^{132}Ce	1.181	0.024	0.638
^{126}Ba	1.120	0.019	0.375	^{133}Ce	1.627	0.032	0.646
^{127}Ba	1.750	0.029	0.525	^{134}Ce	1.716	0.036	0.707
^{128}Ba	2.072	0.036	0.713	^{135}Ce	1.887	0.040	0.718
^{129}Ba	2.707	0.046	0.874	^{136}Ce	1.793	0.041	0.675
^{130}Ba	2.968	0.052	0.975	^{137}Ce	2.280	0.054	0.602
^{131}Ba	3.550	0.063	0.975	^{138}Ce	2.204	0.055	0.564
^{132}Ba	3.919	0.074	1.053	^{139}Ce	2.127	0.054	0.508
^{133}Ba	3.899	0.079	0.966	^{140}Ce	2.109	0.054	0.499
^{134}Ba	4.302	0.085	1.063	^{141}Ce	1.774	0.049	0.403
^{135}Ba	3.729	0.077	0.873	^{142}Ce	1.470	0.046	0.336
^{136}Ba	3.508	0.071	0.825	^{143}Ce	1.369	0.039	0.358
^{137}Ba	3.654	0.073	0.839	^{144}Ce	1.251	0.038	0.137
^{138}Ba	3.739	0.073	0.854	^{145}Ce	1.506	0.046	0.169
^{139}Ba	3.354	0.075	0.364	^{146}Ce	1.496	0.033	0.167
^{140}Ba	3.744	0.071	0.405	^{147}Ce	1.373	0.027	0.151
^{141}Ba	3.508	0.049	0.381	^{148}Ce	1.083	0.019	0.118
^{142}Ba	3.914	0.044	0.426	^{149}Ce	0.763	0.015	0.083
^{143}Ba	3.240	0.033	0.352	^{150}Ce	0.463	0.011	0.056
^{144}Ba	2.517	0.024	0.303	^{151}Ce	0.043	0.002	0.011
^{145}Ba	0.755	0.010	0.174	^{152}Ce	0.015	0.001	0.005
^{146}Ba	0.350	0.006	0.081	^{128}Pr	0.023	0.002	0.005
^{147}Ba	0.060	0.001	0.016	^{129}Pr	0.052	0.002	0.013
^{148}Ba	0.014	0.001	0.004	^{130}Pr	0.129	0.004	0.052
^{124}La	0.037	0.002	0.013	^{131}Pr	0.349	0.009	0.097
^{125}La	0.110	0.003	0.027	^{132}Pr	0.623	0.014	0.203
^{126}La	0.307	0.008	0.082	^{133}Pr	0.882	0.019	0.353
^{127}La	0.530	0.011	0.164	^{134}Pr	1.145	0.024	0.454
^{128}La	1.043	0.019	0.274	^{135}Pr	0.962	0.022	0.582
^{129}La	1.136	0.022	0.422	^{136}Pr	1.330	0.030	0.571
^{130}La	1.520	0.029	0.584	^{137}Pr	1.160	0.029	0.584
^{131}La	1.771	0.035	0.611	^{138}Pr	1.365	0.034	0.534
^{132}La	2.417	0.046	0.719	^{139}Pr	1.419	0.038	0.474
^{133}La	2.447	0.050	0.718	^{140}Pr	1.859	0.049	0.484
^{134}La	2.842	0.058	0.797	^{141}Pr	1.616	0.046	0.397
^{135}La	2.759	0.061	0.731	^{142}Pr	1.447	0.044	0.342
^{136}La	2.811	0.065	0.683	^{143}Pr	1.290	0.042	0.305
^{137}La	2.652	0.062	0.622	^{144}Pr	1.209	0.042	0.278
^{138}La	2.456	0.058	0.564	^{145}Pr	1.192	0.042	0.273
^{139}La	2.583	0.059	0.592	^{146}Pr	1.046	0.036	0.114
^{140}La	2.078	0.054	0.474	^{147}Pr	0.835	0.033	0.092

TABLE XV: Isotopic cross-sections of spallation-evaporation fragments of ^{238}U(1A GeV)+d, with their statistical and systematic uncertainties.

nucleus	σ (mb)	ε_{STAT} (mb)	ε_{SYST} (mb)	nucleus	σ (mb)	ε_{STAT} (mb)	ε_{SYST} (mb)
^{148}Pr	0.794	0.029	0.088	^{157}Pm	0.007	0.001	0.002
^{149}Pr	0.819	0.023	0.091	^{158}Pm	0.003	0.001	0.001
^{150}Pr	0.725	0.020	0.080	^{145}Sm	0.619	0.022	0.401
^{151}Pr	0.563	0.015	0.062	^{146}Sm	0.448	0.017	0.356
^{152}Pr	0.210	0.007	0.023	^{147}Sm	0.620	0.025	0.196
^{153}Pr	0.099	0.005	0.012	^{148}Sm	0.489	0.022	0.158
^{154}Pr	0.008	0.001	0.003	^{149}Sm	0.623	0.028	0.146
^{131}Nd	0.033	0.002	0.013	^{150}Sm	0.420	0.020	0.109
^{132}Nd	0.080	0.003	0.038	^{151}Sm	0.336	0.018	0.084
^{133}Nd	0.254	0.007	0.095	^{152}Sm	0.362	0.020	0.096
^{134}Nd	0.450	0.011	0.210	^{153}Sm	0.276	0.017	0.076
^{135}Nd	0.662	0.016	0.346	^{154}Sm	0.233	0.016	0.057
^{136}Nd	0.906	0.021	0.458	^{155}Sm	0.153	0.013	0.037
^{137}Nd	0.988	0.023	0.593	^{156}Sm	0.114	0.010	0.026
^{138}Nd	0.992	0.025	0.656	^{157}Sm	0.050	0.005	0.012
^{139}Nd	1.061	0.028	0.560	^{158}Sm	0.033	0.004	0.009
^{140}Nd	0.867	0.026	0.598	^{159}Sm	0.018	0.003	0.006
^{141}Nd	1.143	0.033	0.431	^{160}Sm	0.009	0.002	0.004
^{142}Nd	1.145	0.035	0.363	^{148}Eu	0.419	0.020	0.308
^{143}Nd	1.182	0.039	0.297	^{149}Eu	0.437	0.021	0.229
^{144}Nd	1.034	0.037	0.244	^{150}Eu	0.433	0.022	0.144
^{145}Nd	0.951	0.035	0.220	^{151}Eu	0.336	0.019	0.107
^{146}Nd	0.813	0.033	0.193	^{152}Eu	0.372	0.021	0.089
^{147}Nd	0.696	0.031	0.168	^{153}Eu	0.300	0.019	0.074
^{148}Nd	0.666	0.030	0.163	^{154}Eu	0.314	0.021	0.067
^{149}Nd	0.568	0.025	0.130	^{155}Eu	0.194	0.014	0.043
^{150}Nd	0.481	0.023	0.052	^{156}Eu	0.185	0.014	0.040
^{151}Nd	0.550	0.022	0.058	^{157}Eu	0.087	0.009	0.019
^{152}Nd	0.358	0.014	0.038	^{158}Eu	0.044	0.006	0.010
^{153}Nd	0.262	0.011	0.029	^{159}Eu	0.031	0.004	0.007
^{154}Nd	0.141	0.007	0.020	^{160}Eu	0.014	0.002	0.003
^{155}Nd	0.076	0.005	0.010	^{153}Gd	0.316	0.018	0.095
^{156}Nd	0.005	0.001	0.001	^{154}Gd	0.201	0.014	0.090
^{133}Pm	0.027	0.002	0.007	^{155}Gd	0.231	0.016	0.065
^{134}Pm	0.069	0.003	0.018	^{156}Gd	0.164	0.013	0.044
^{135}Pm	0.181	0.006	0.060	^{157}Gd	0.149	0.014	0.033
^{136}Pm	0.410	0.012	0.142	^{158}Gd	0.092	0.011	0.020
^{137}Pm	0.516	0.014	0.262	^{159}Gd	0.079	0.009	0.017
^{138}Pm	0.909	0.022	0.393	^{160}Gd	0.042	0.005	0.009
^{139}Pm	0.634	0.018	0.555	^{161}Gd	0.017	0.003	0.004
^{140}Pm	0.843	0.022	0.630	^{162}Gd	0.009	0.002	0.002
^{141}Pm	0.469	0.016	0.413	^{152}Tb	0.098	0.002	0.037
^{142}Pm	0.979	0.028	0.560	^{153}Tb	0.131	0.004	0.038
^{143}Pm	0.774	0.024	0.499	^{154}Tb	0.168	0.005	0.037
^{144}Pm	0.870	0.030	0.341	^{155}Tb	0.165	0.006	0.023
^{145}Pm	0.830	0.032	0.242	^{156}Tb	0.183	0.011	0.020
^{146}Pm	0.792	0.031	0.215	^{157}Tb	0.184	0.008	0.017
^{147}Pm	0.777	0.031	0.188	^{158}Tb	0.162	0.009	0.014
^{148}Pm	0.606	0.027	0.143	^{159}Tb	0.100	0.009	0.009
^{149}Pm	0.511	0.024	0.114	^{160}Tb	0.067	0.005	0.006
^{150}Pm	0.499	0.024	0.110	^{161}Tb	0.022	0.007	0.003
^{151}Pm	0.484	0.025	0.108	^{154}Dy	0.041	0.001	0.019
^{152}Pm	0.336	0.020	0.074	^{155}Dy	0.088	0.002	0.031
^{153}Pm	0.326	0.020	0.037	^{156}Dy	0.123	0.004	0.029
^{154}Pm	0.254	0.016	0.028	^{157}Dy	0.153	0.005	0.026
^{155}Pm	0.172	0.012	0.018	^{158}Dy	0.144	0.008	0.017
^{156}Pm	0.094	0.007	0.010	^{159}Dy	0.151	0.006	0.014

TABLE XVI: Isotopic cross-sections of spallation-evaporation fragments of ^{238}U(1A GeV)+d, with their statistical and systematic uncertainties.

nucleus	σ (mb)	ε_{STAT} (mb)	ε_{SYST} (mb)
^{160}Dy	0.140	0.008	0.012
^{161}Dy	0.120	0.010	0.010
^{162}Dy	0.064	0.005	0.006
^{163}Dy	0.037	0.005	0.003
^{155}Ho	0.086	0.002	0.056
^{156}Ho	0.126	0.003	0.066
^{157}Ho	0.167	0.004	0.067
^{158}Ho	0.182	0.005	0.049
^{159}Ho	0.190	0.006	0.035
^{160}Ho	0.152	0.008	0.018
^{161}Ho	0.148	0.006	0.015
^{162}Ho	0.109	0.007	0.010
^{163}Ho	0.099	0.009	0.009
^{164}Ho	0.062	0.005	0.005
^{165}Ho	0.038	0.005	0.003
^{161}Er	0.043	0.001	0.012
^{162}Er	0.065	0.003	0.011
^{163}Er	0.082	0.003	0.010
^{164}Er	0.074	0.006	0.007
^{165}Er	0.059	0.009	0.005
^{166}Er	0.043	0.005	0.004
^{167}Er	0.023	0.004	0.002
^{165}Tm	0.005	0.000	0.001
^{166}Tm	0.032	0.002	0.004
^{167}Tm	0.049	0.005	0.004
^{168}Tm	0.047	0.006	0.004
^{169}Tm	0.028	0.004	0.003

TABLE XVII: Isotopic cross-sections of spallation-evaporation fragments of ^{238}U(1A GeV)+d, with their statistical and systematic uncertainties.

E. Casarejos, S. Czajkowski, T. Enqvist, S. Leray, P. Napolitani, J. Pereira, F. Rejmund, M.-V. Ricciardi, K.-H. Schmidt, C. Stephan, J. Taíeb, L. Tassan-Got and C. Volant, Phys. Rev. Lett. 93 (2004) 212701

[20] C. Villagrasa, A. Boudard, J.E. Ducret, B. Fernández-Rodríguez, S. Leray, C. Volant, W. Wlazlo, P. Armbruster, T. Enqvist, F. Hammache, K. Helariutta, B. Jurado, M. V. Ricciardi, K.-H. Schmidt, K Sümmerer, F. Vives, O. Yordanov, L. Audouin, L. Ferran, F. Rejmund, C. Stéphan, L. Tassan-Got, J. Benlliure, E. Casarejos, M. Fernández, J. Pereira, S. Czajkowski, D. Karamanis, M. Pravikoff, J. George, R.A. Mewaldt, N. Yanazak, A. Wiedenbeck, J. Connel, T. Faestermann, A. Heinz and A. Junghans, AIP Conference Proceedings, Vol.769 (2005) 842

[21] B. Fernández-Rodríguez, P. Armbruster, L. Audouin, J. Benlliure, M. Bernas, A. Boudard, E. Casarejos, S. Czajkowski, J.E. Ducret, T. Enqvist, B. Jurado, R. Legrain, S. Leray, B. Mustapha, J. Pereira, M. Pravikoff, F. Rejmund, M. V. Ricciardi, K.-H. Schmidt, C. Stéphan, J. Taíeb and L. Tassan-Got and C. Volant, Nucl. Phys. A747 (2005) 227

[22] M. Bernas, P. Armbruster, J. Benlliure, A. Boudard, E. Casarejos, S. Czajkowski, T. Enqvist, R. Legrain, S. Leray, B. Mustapha, P. Napolitani, J. Pereira, F. Rejmund, M. V. Ricciardi, K.-H. Schmidt, C. Stéphan, J. Taíeb, L. Tassan-Got, C. Volant and W. Wlazlo, Nucl.

Phys. A765 (2006) 197

[23] M. V. Ricciardi, P. Armbruster, J. Benlliure, M. Bernas, A. Boudard, S. Czajkowski, T. Enqvist, A. Kelić, R. Legrain, S. Leray, B. Mustapha, J. Pereira, F. Rejmund, K.-H. Schmidt, C. Stéphan, L. Tassan-Got, C. Volant and O. Yordanov, Phys. Rev. C73 (2006) 014607

[24] C. Rubbia et al., Rep. CERN-AT/95-44(ET) (1995)

[25] C.D.Bowman, Ann. Rev. Nucl. Part. Sci. 48 (1998) 505

[26] http://www.gsi.de

[27] M. Steiner et al., M. Blasche, H.-G. Clerc, H. Eickhoff, B. Franczak, H. Geissel, G. Münzenberg, K.-H. Schmidt, H. Stelzer and K. Sümmerer, Nucl. Instr. and Meth. A312 (1992) 420

[28] R. Anne, A. Lefol, G. Milleret and R. Perret, Nucl. Instr. and Meth. 152 (1985) 395

[29] B. Jurado, K.-H. Schmidt and K.-H. Behr, Nucl. Instr. and Meth. A478 (2002) 493

[30] Ph. Chesny, A. Forgeas, J.M. Gheller, G. Guiller, P. Pariset, L. Tassan-Got, P. Armbruster, K.-H. Behr, J. Benlliure, K. Burkard, A. Brünle, T. Enqvist, F. Farget, K.-H. Schmidt, GSI-reports LNS/SSGD/93-73

[31] H. Geissel et al., P. Armbruster, K.H. Behr, A. Brünle, K. Burkard, M. Chen, H. Folger, B. Franczak, H. Keller, O. Klepper, B. Langenbeck, F. Nickel, E. Pfeng, M. Pfützner, E. Roeckl, K. Rykaczewski, I. Schall, D. Schardt, C. Scheidenberger, K.H. Schmidt, A. Schröter, T. Schwab, K. Sümmerer, M. Weber, G. Münzenberg, T. Brohm, H.-G. Clerc, M. Fauerbach, J.-J. Gaimard, A. Grewe, E. Hanelt, B. Knödler, M. Steiner, B. Voss, J. Weckenmann, C. Ziegler, A. Magel, H. Wollnik, J.P. Dufour, Y. Fujita, D.J. Vieira and B. Sherrill, Nucl. Instr. and Meth. B70 (1992) 286

[32] B. Voss, T. Brohm, H.-G. Clerc, A. Grewe, E. Hanelt, A. Heinz, M. de Jong, A. Junhans, W. Morawek, C. Röhl, S. Steinhäuser, C. Ziegler, K.-H. Schmidt, K.-H. Behr, H. Geissel, G. Münzenberg, F. Nickel, C. Scheidenberger, K. Sümmerer, A. Magel and M. Pfützner Nucl. Instr. and Meth. A364 (1995) 150.

[33] M. Pfützner, H. Geissel, G. Münzenberg, F. Nickel, C. Scheidenberger, K.-H. Schmidt, K. Sümmerer, T. Brohm, B. Voss and H. Bichsel, Nucl. Instr. and Meth. B86 (1994) 213

[34] H. Stelzer, Nucl. Instr. and Meth. A310 (1991) 103

[35] J. Benlliure, J. Pereira and K.-H. Scmidt, Nucl. Instr. Meth. A478 (2002) 493

[36] J. Pereira, J. Benlliure and K.-H. Schmidt, Nucl. Instr. and Meth. B204 (2003) 517

[37] P. Karol, Phys. Rev. C11, 4 (1975) 1203

[38] J.-J. Gaimard, K.-H. Schmidt Nucl. Phys. A531 (1991) 709

[39] P. Napolitani, L. Tassan-Got, P. Armbruster and M. Bernas, Nucl. Phys. A727 (2003) 120

[40] T. Enqvist, J. Benlliure, F. Farget, K.-H. Schmidt, P. Armbruster, M. Bernas, L. Tassan-Got, A. Boudard, R. Legrain, C. Volant, C. Böeckstiegel, M. de Jong and J.P. Dufour, Nucl. Phys. A658 (1999) 47

[41] C. Scheidenberger, Th. Stoehlker, W.E. Meyerhof, H. Geissel, P.H. Mokler and B. Blank Nucl. Instr. Methods B142 (1998) 441

[42] The GLOBAL program is available via anonymous ftp from borsu8.in2p3.fr in the directory $/pub/nex/global/pc$ and $/pub/nex/global/vms_unix$ for PCs and workstations, respectively

[43] R. Serber, Phys. Rev. 72 (1947) 1114

[44] J. Benlliure, A. Grewe, M. de Jong, K.-H. Schmidt and S. Zhdanov Nucl. Phys. A 628 (1998) 458

[45] B.D. Wilkins, E.P. Steinberg and R.R. Chasman., Phys. Rev. C14 (1976) 1832

[46] The EXFOR entries are available at the OECD NEA Data Bank, http://www.nea.fr/html/dbdata

[47] P.C. Stevenson, H.G. Hicks, W.E. Nervik and D.R. Nethaway, Phys. Rev. 111 (1958) 886

[48] A.V. Prokofiev, Nucl. Instr. and Meth. A463 (2001) 557

[49] F. Vives, private communication